

# AdaWAC: Adaptively Weighted Augmentation Consistency Regularization for Volumetric Medical Image Segmentation

Yijun Dong<sup>\*1</sup>, Yuege Xie<sup>\*†2</sup>, and Rachel Ward<sup>1</sup>

<sup>1</sup>The University of Texas at Austin

<sup>2</sup>Snap Inc.

October 6, 2022

## Abstract

Sample reweighting is an effective strategy for learning from training data coming from a mixture of subpopulations. In volumetric medical image segmentation, the data input are similarly distributed, but the associated data labels fall into two subpopulations—“label-sparse” and “label-dense”—depending on whether the data image occurs near the beginning/end of the volumetric scan or the middle. Existing reweighting algorithms have focused on hard- and soft- thresholding of the label-sparse data, which results in loss of information and reduced sample efficiency by discarding valuable data input. For this setting, we propose *AdaWAC* as an adaptive weighting algorithm that introduces a set of trainable weights which, at the saddle point of the underlying objective, assigns label-dense samples to supervised cross-entropy loss and label-sparse samples to unsupervised consistency regularization. We provide a convergence guarantee for *AdaWAC* by recasting the optimization as online mirror descent on a saddle point problem. Moreover, we empirically demonstrate that *AdaWAC* not only enhances segmentation performance and sample efficiency but also improves robustness to the subpopulation shift in labels.

## 1 Introduction

Modern machine learning is revolutionizing the field of medical imaging, especially in computer-aided diagnosis with Computed Tomography (CT) and Magnetic Resonance Imaging (MRI) scans. While classical learning algorithms (*e.g.*, empirical risk minimization) are sensitive to the assumption that the training samples are independently and identically distributed (*i.i.d.*), real-world volumetric medical images rarely fit in this framework. In efforts to go beyond *i.i.d.* samples, numerous algorithms [Sagawa et al., 2020, Yeung et al., 2022] have been proposed to improve distributional robustness of learning in different settings. Specifically for medical image segmentation, as instantiated in Figure 1, the segmentation labels corresponding to different cross-sections of organs within a given volume tend to have distinct distributions. That is, the slices toward the beginning/end of the volume that contain no target organs have very few, if any, segmentation labels (which we refer to as “label-sparse”); whereas segmentation labels are prolific in the slices toward the middle of the volume (“label-dense”). Such discrepancy in labels results in distinct difficulty levels measured by the training cross-entropy [Wang et al., 2021b] and leads to various training

<sup>\*</sup>Equal contribution. Correspondence to: [ydong@utexas.edu](mailto:ydong@utexas.edu)

<sup>†</sup>Work done at University of Texas at Austin.

schedulers [Hacohen and Weinshall, 2019, Tang et al., 2018, Tullis and Benjamin, 2011]. Motivated by the separation between label-sparse and label-dense samples, we explore the following questions in this work:

*What is the effect of separation between sparse and dense labels on segmentation?*  
*Can we leverage such separation to improve the segmentation accuracy?*

We first formulate a model for the mixture of label-sparse and label-dense samples in volumetric medical imaging as a subpopulation shift in the conditional distribution of labels given images  $P(y|x)$ . As illustrated in Figure 1, such subpopulation shift induces a separation in supervised cross-entropy between sparse and dense labels, even though the data image distribution ( $P(x)$ ) remains roughly uniform.

Prior work addressing the issue of subpopulation shift has focused on hard thresholding the loss to discard label-sparse samples. These works include the Trimmed Loss Estimator [Shen and Sanghavi, 2019], MKL-SGD [Shah et al., 2020], Ordered SGD [Kawaguchi and Lu, 2020], and the quantile-based Kacmarz algorithm [Haddock et al., 2020]. However, by completely discarding the samples from some subpopulations (e.g. samples with label corruption estimated by their losses) at each iteration, information in the discarded data is lost, and sample efficiency is reduced. To incorporate the information from both subpopulations, the papers [Sagawa et al., 2020, Wang et al., 2018] propose to relax the hard thresholding operation to soft thresholding. However, diminishing the weights assigned to subpopulations of data according to the properties of their labels reduces the importance of the data and labels *simultaneously*. This is still not ideal, and suggests that learning efficiency may be further improved by exploiting the uniformity of data and the separation of labels separately.

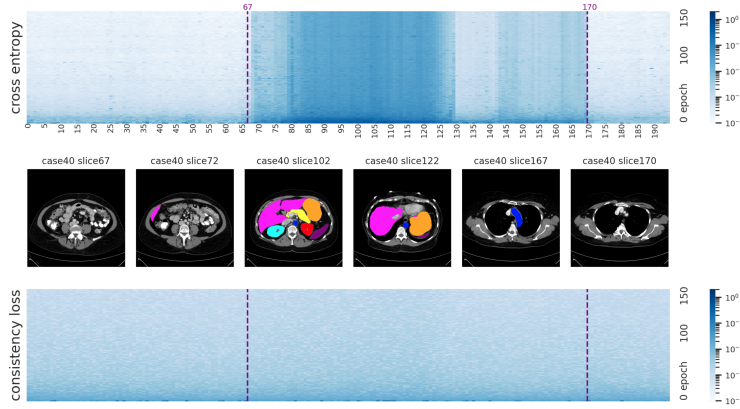


Figure 1: Evolution of cross-entropy losses versus consistency regularization terms for slices across one training volume (Case 40) in the Synapse dataset (Section 5) during training.

Instead of thresholding or down-weighting the label-sparse samples, we propose to incorporate the image inputs to these samples via *augmentation consistency regularization*. Consistency regularization [Bachman et al., 2014, Laine and Aila, 2016, Sohn et al., 2020] aims to learn the proximity  $d(x, x')$  between data augmentations corresponding to the same samples  $x \sim x'$  (e.g.,  $x'$  is a rotation of  $x$ ); consistency regularization has become a powerful strategy for utilizing unlabeled data recently. For medical imaging tasks, consistency regularization has been extensively studied in the semi-supervised learning setting [Basak et al., 2022, Bortsova et al., 2019, Li et al., 2020, Wang et al., 2021a, Zhang et al., 2021, Zhao et al., 2019, Zhou et al., 2021]. In contrast to these works, we will explore the potency of consistency regularization in the *fully supervised setting*—leveraging the spare information in all image inputs, regardless of their label subpopulations.

In light of the uniformity of unsupervised consistency on different slices through a particular volume, the augmentation consistency of the encoder layer outputs serves as a natural reference for separating samples from different subpopulations. In light of this observation, we introduce the *weighted augmentation consistency (WAC) regularization*—a minimax formulation that not only incorporates consistency regularization but also leverages this consistency regularization as a reference for reweighting the cross-entropy and the augmentation consistency terms corresponding to different samples. At the saddle point of our minimax formulation, the WAC regularization automatically separates samples from different label subpopulations by assigning all weight to the consistency terms for label-sparse samples, and all weight to the cross-entropy terms for label-dense samples.

We further introduce *AdaWAC*, an algorithm for solving the minimax problem posed by the WAC regularization, corresponding to a mirror-descent-based adaptive weighting scheme for distributionally-robust optimization [Sagawa et al., 2020]. By adaptively adjusting the weights between the cross-entropy and consistency terms of different samples, *AdaWAC* comes with both convergence guarantees and empirical success.

The main contributions of this work are summarized as follows:

- We cast the discrepancy between the sparse and dense labels within each volume as subpopulation shift in the conditional distribution  $P(y|x)$ .
- We propose WAC regularization which uses the consistency of encoder layer outputs (in a UNet-style architecture) as a natural reference to incentivize separation between samples with sparse and dense labels, along with an adaptive weighting algorithm—*AdaWAC*—for solving the WAC regularization problem with a convergence guarantee.
- Through extensive numerical experiments on benchmark volumetric medical imaging data, we demonstrate the power of *AdaWAC* not only for enhancing segmentation performance and sample efficiency but also for improving robustness to the subpopulation shift in labels.

## 1.1 Related Work

**Sample reweighting.** Sample reweighting is a popular strategy for dealing with subpopulation shifts in training data where different weights are assigned to samples from different subpopulations. In particular, the distributionally-robust optimization (DRO) framework [Ben-Tal et al., 2013, Duchi and Namkoong, 2018, Duchi et al., 2016, Sagawa et al., 2020] considers a collection of training sample groups from different distributions. With the explicit grouping of samples, the goal is to minimize the worst-case loss over the groups. Without prior knowledge on sample grouping, importance sampling [Alain et al., 2015, Gopal, 2016, Katharopoulos and Fleuret, 2018, Loshchilov and Hutter, 2015, Needell et al., 2014, Zhao and Zhang, 2015], iterative trimming [Kawaguchi and Lu, 2020, Shen and Sanghavi, 2019], and empirical-loss-based reweighting [Wu et al., 2022] are commonly incorporated in the stochastic optimization process for adaptive reweighting and separation of samples from different subpopulations.

**Consistency regularization.** Consistency regularization [Bachman et al., 2014, Laine and Aila, 2016, Sohn et al., 2020] is a popular way to exploit data augmentations. Consistency regularization encourages the model to learn the vicinity among augmentations of the same sample based on the observation that data augmentations generally preserve the semantic information in data.

For medical imaging, consistency regularization is generally leveraged as a semi-supervised learning tool [Basak et al., 2022, Bortsova et al., 2019, Li et al., 2020, Wang et al., 2021a, Zhang et al., 2021, Zhao et al., 2019, Zhou et al., 2021]. In efforts to incorporate consistency regularization in medical image segmentation with augmentation-sensitive labels, Li et al. [2020] encourages transformation consistency between predictions with augmentations applied to the image

inputs and the segmentation outputs. Basak et al. [2022] penalizes inconsistent segmentation outputs between teacher-student models, with MixUp [Zhang et al., 2017] applied on image inputs of the teacher model and segmentation outputs of the student model. Instead of enforcing consistency in the segmentation output space as above, our algorithm leverages the insensitivity of sparse labels to augmentations and encourages consistent encodings (in the latent space of encoder outputs) on label-sparse samples.

## 2 Problem Setup

**Notation.** For any  $K \in \mathbb{N}$ , we denote  $[K] = \{1, \dots, K\}$ . We represent the elements and subtensors of an arbitrary tensor by adapting the syntax for Python slicing on the subscript (except counting from 1). For example,  $\mathbf{x}_{[i,j]}$  denotes the  $(i, j)$ -entry of the two-dimensional tensor  $\mathbf{x}$ , and  $\mathbf{x}_{[i,:]}$  denotes the  $i$ -th row. Let  $\mathbb{I}$  be a function onto  $\{0, 1\}$  such that, for any event  $e$ ,  $\mathbb{I}\{e\} = 1$  if  $e$  is true and 0 otherwise. For any distribution  $P$  and  $n \in \mathbb{N}$ , we let  $P^n$  denote the joint distribution of  $n$  samples drawn *i.i.d.* from  $P$ . Finally, we say that an event happens with high probability (*w.h.p.*) if the event takes place with probability  $1 - \Omega(\text{poly}(n))^{-1}$ .

### 2.1 Pixel-wise Classification with Sparse and Dense Labels

We consider the volumetric medical image segmentation as a pixel-wise multi-class classification problem where we aim to learn a pixel-wise classifier  $h : \mathcal{X} \rightarrow [K]^d$  that serves as a good approximation to the ground truth  $h^* : \mathcal{X} \rightarrow [K]^d$ .

Recall as illustrated in Figure 1 that separation in cross-entropy loss values between samples with different fractions of non-background labels becomes apparent during training. We refer to a sample  $(\mathbf{x}, \mathbf{y}) \in \mathcal{X} \times [K]^d$  as *label-sparse* if most pixels in  $\mathbf{y}$  are labeled as background; for these samples, the cross-entropy loss on  $(\mathbf{x}, \mathbf{y})$  converges rapidly in the early stage of training. Otherwise, we say that  $(\mathbf{x}, \mathbf{y})$  is *label-dense*. Formally, we describe such variation as a subpopulation shift in the label distribution.

**Definition 1** (Mixture of label-sparse and label-dense distributions). We assume that *label-sparse* and *label-dense* samples have distributions  $P_0$  and  $P_1$  with distinct conditional distributions  $P_0(\mathbf{y}|\mathbf{x})$  and  $P_1(\mathbf{y}|\mathbf{x})$  but common marginal distribution  $P(\mathbf{x})$  such that  $P_i(\mathbf{x}, \mathbf{y}) = P_i(\mathbf{y}|\mathbf{x})P(\mathbf{x})$  ( $i = 0, 1$ ). For  $\xi \in [0, 1]$ , we define a data distribution  $P_\xi$  where each sample  $(\mathbf{x}, \mathbf{y}) \sim P_\xi$  is drawn either from  $P_1$  with probability  $\xi$  or from  $P_0$  with probability  $1 - \xi$ .

We aim to learn a pixel-wise classifier from a function class  $\mathcal{H} \ni h_\theta = \arg\max_{k \in [K]} f_\theta(\mathbf{x})_{[j,:]}$  for all  $j \in [d]$  where the underlying function  $f_\theta \in \mathcal{F}$ , parameterized by some  $\theta \in \mathcal{F}_\theta$ , admits an encoder-decoder structure:

$$\mathcal{F} = \left\{ f_\theta = \phi_\theta \circ \psi_\theta \mid \phi_\theta : \mathcal{X} \rightarrow \mathcal{Z}, \psi_\theta : \mathcal{Z} \rightarrow [0, 1]^{d \times K} \right\}. \quad (1)$$

Here  $\phi_\theta, \psi_\theta$  correspond to the encoder and decoder functions, respectively. The parameter space  $\mathcal{F}_\theta$  is equipped with the norm  $\|\cdot\|_{\mathcal{F}}$  and its dual norm  $\|\cdot\|_{\mathcal{F},*}$ <sup>1</sup>.  $(\mathcal{Z}, \varrho)$  is a latent metric space.

To learn from segmentation labels, we consider the *averaged cross-entropy loss*:

$$\ell_{CE}(\theta; (\mathbf{x}, \mathbf{y})) = -\frac{1}{d} \sum_{j=1}^d \sum_{k=1}^K \mathbb{I}\{\mathbf{y}_{[j]} = k\} \cdot \log(f_\theta(\mathbf{x})_{[j,k]}) = -\frac{1}{d} \sum_{j=1}^d \log(f_\theta(\mathbf{x})_{[j, \mathbf{y}_{[j]}]}). \quad (2)$$

<sup>1</sup>For AdaWAC (Proposition 2 in Section 4),  $\mathcal{F}_\theta$  is simply a subspace in the Euclidean space with dimension equal to the total number of parameters for each  $\theta \in \mathcal{F}_\theta$ , with  $\|\cdot\|_{\mathcal{F}}$  and  $\|\cdot\|_{\mathcal{F},*}$  both being the  $\ell_2$ -norm.



We assume the proper learning setting: there exists  $\theta^* \in \bigcap_{\xi \in [0,1]} \operatorname{argmin}_{\theta \in \mathcal{F}_\theta} \mathbb{E}_{(\mathbf{x}, \mathbf{y}) \sim P_\xi} [\ell_{CE}(\theta; (\mathbf{x}, \mathbf{y}))]$ , which is invariant with respect to  $\xi$ .<sup>2</sup>

## 2.2 Augmentation Consistency Regularization

Despite the invariance of  $f_{\theta^*}$  to  $P_\xi$  on the population loss, in practice we have a finite number of training samples and the predominance of label-sparse samples in the training set introduces difficulties due to the class imbalances. As an extreme scenario for the pixel-wise classifier with encoder-decoder structure (Equation (1)), when the label-sparse samples are predominant ( $\xi \ll 1$ ), a decoder function  $\psi_\theta$  that predicts every pixel as background can achieve near-optimal cross-entropy loss, regardless of the encoder function  $\phi_\theta$ , considerably compromising the test performance (cf. Table 1). To encourage legit encoding even in the absence of sufficient dense labels, we leverage the unsupervised consistency regularization on the *encoder function*  $\phi_\theta$  based on data augmentations.

Let  $\mathcal{A}$  be a distribution over transformations on  $\mathcal{X}$  where for any  $\mathbf{x} \in \mathcal{X}$ , each  $A \sim \mathcal{A}$  ( $A : \mathcal{X} \rightarrow \mathcal{X}$ ) induces an augmentation  $A(\mathbf{x})$  of  $\mathbf{x}$  that perturbs low-level information in  $\mathbf{x}$ . We aim to learn an encoder function  $\phi_\theta : \mathcal{X} \rightarrow \mathcal{Z}$  that is capable of filtering out low-level information from  $\mathbf{x}$  and therefore provides similar encodings for augmentations of the same sample. Recalling the metric  $\varrho$  (e.g., the Euclidean distance) on  $\mathcal{Z}$ , for a given scaling hyperparameter  $\lambda_{AC} > 0$ , we measure the similarity between augmentations with a consistency regularization term on  $\phi_\theta(\cdot)$ : for any  $A_1, A_2 \sim \mathcal{A}^2$ ,

$$\ell_{AC}(\theta; \mathbf{x}, A_1, A_2) \triangleq \lambda_{AC} \cdot \varrho(\phi_\theta(A_1(\mathbf{x})), \phi_\theta(A_2(\mathbf{x}))). \quad (3)$$

For the  $n$  training samples  $\{(\mathbf{x}_i, \mathbf{y}_i)\}_{i \in [n]} \sim P_\xi^n$ , we consider  $n$  pairs of data augmentation transformations  $\{(A_{i,1}, A_{i,2})\}_{i \in [n]} \sim \mathcal{A}^{2n}$ . In the basic version, we encourage the similar encoding  $\phi_\theta(\cdot)$  of the augmentation pairs  $(A_{i,1}(\mathbf{x}_i), A_{i,2}(\mathbf{x}_i))$  for all  $i \in [n]$  via consistency regularization:

$$\min_{\theta \in \mathcal{F}_{\theta^*}(\gamma)} \frac{1}{n} \sum_{i=1}^n \ell_{CE}(\theta; (\mathbf{x}_i, \mathbf{y}_i)) + \ell_{AC}(\theta; \mathbf{x}_i, A_{i,1}, A_{i,2}). \quad (4)$$

We enforce consistency on  $\phi_\theta(\cdot)$  in light of the encoder-decoder architecture: the encoder is generally designed to abstract essential information and filters out low-level non-semantic perturbations (e.g., those introduced by augmentations), while the decoder recovers the low-level information for the pixel-wise classification. Therefore, with different  $A_1, A_2 \sim \mathcal{A}$ , the encoder output  $\phi_\theta(\cdot)$  tends to be more consistent than the other intermediate layers, especially for label-dense samples.

## 3 Weighted Augmentation Consistency (WAC) Regularization

As the motivation, we begin with a key observation about the averaged cross-entropy:

*Remark 1* (Separation of averaged cross-entropy loss on  $P_0$  and  $P_1$ ). As demonstrated in Figure 1, the sparse labels from  $P_0$  tend to be much easier to learn than the dense ones from  $P_1$ , leading

<sup>2</sup>We assume proper learning only to (i) highlight the invariance of the desired ground truth to  $\xi$  that can be challenging to learn with finite samples in practice and (ii) provide a natural pivot for the convex and compact neighborhood  $\mathcal{F}_{\theta^*}(\gamma)$  of ground truth  $\theta^*$  in Assumption 1 granted by the pretrained initialization, where  $\theta^*$  can also be replaced with the pretrained initialization weights  $\theta_0 \in \mathcal{F}_{\theta^*}(\gamma)$ . In particular, neither our theory nor the *AdaWAC* algorithm requires the function class  $\mathcal{F}$  to be expressive enough to truly contain such  $\theta^*$ .

to considerable separation of averaged cross-entropy losses on the sparse and dense labels after a sufficient number of training epochs. Precisely,  $\ell_{CE}(\theta; (\mathbf{x}, \mathbf{y})) \ll \ell_{CE}(\theta; (\mathbf{x}', \mathbf{y}'))$  for most label-sparse samples  $(\mathbf{x}, \mathbf{y}) \sim P_0$  and label-dense samples  $(\mathbf{x}', \mathbf{y}') \sim P_1$ .

Although Equation (4) with consistency regularization alone can boost the segmentation accuracy during testing (*cf.* Table 4), it does not take the separation between label-sparse and label-dense samples into account. In Section 5, we will empirically demonstrate that proper exploitation of such separation, like the formulation introduced below, can lead to improved classification performance.

We can formalize the notion of separation between  $P_0$  and  $P_1$  based on the consistency regularization term (Equation (3)) with the following assumption<sup>3</sup>.

**Assumption 1** (*n*-separation between  $P_0$  and  $P_1$ ). Given a sufficiently small  $\gamma > 0$ , let  $\mathcal{F}_{\theta^*}(\gamma) = \{\theta \in \mathcal{F}_\theta \mid \|\theta - \theta^*\|_{\mathcal{F}} \leq \gamma\}$  be a compact and convex neighborhood of well-trained pixel-wise classifiers<sup>4</sup>. We say that  $P_0$  and  $P_1$  are *n-separated over  $\mathcal{F}_{\theta^*}(\gamma)$*  if there exists  $\omega > 0$  such that with probability  $1 - \Omega(n^{1+\omega})^{-1}$  over  $((\mathbf{x}, \mathbf{y}), (A_1, A_2)) \sim P_\xi \times \mathcal{A}^2$ , the following hold:

- (i)  $\ell_{CE}(\theta; (\mathbf{x}, \mathbf{y})) < \ell_{AC}(\theta; \mathbf{x}, A_1, A_2)$  for all  $\theta \in \mathcal{F}_{\theta^*}(\gamma)$  given  $(\mathbf{x}, \mathbf{y}) \sim P_0$
- (ii)  $\ell_{CE}(\theta; (\mathbf{x}, \mathbf{y})) > \ell_{AC}(\theta; \mathbf{x}, A_1, A_2)$  for all  $\theta \in \mathcal{F}_{\theta^*}(\gamma)$  given  $(\mathbf{x}, \mathbf{y}) \sim P_1$

This assumption is motivated by the empirical observation that the perturbation in  $\phi_\theta(\cdot)$  induced by  $\mathcal{A}$  is more uniform across  $P_0$  and  $P_1$  than the averaged cross-entropy, as instantiated in Figure 3.

Under Assumption 1, up to a proper scaling hyperparameter  $\lambda_{AC}$ , the consistency regularization (Equation (3)) can separate the averaged cross-entropy loss (Equation (2)) on  $n$  label-sparse and label-dense samples with probability  $1 - \Omega(n^\omega)^{-1}$  (as explained formally in Appendix A). In particular, larger  $n$  corresponds to stronger separation between  $P_0$  and  $P_1$ .

With Assumption 1, we introduce a minimax formulation that incentivizes the separation of label-sparse and label-dense samples automatically by introducing a flexible weight  $\beta_{[i]} \in [0, 1]$  that balances  $\ell_{CE}(\theta; (\mathbf{x}_i, \mathbf{y}_i))$  and  $\ell_{AC}(\theta; \mathbf{x}_i, A_{i,1}, A_{i,2})$  for each of the  $n$  samples.

$$\begin{aligned} \hat{\theta}^{WAC}, \hat{\beta} \in \operatorname{argmin}_{\theta \in \mathcal{F}_{\theta^*}(\gamma)} \operatorname{argmax}_{\beta \in [0,1]^n} \left\{ \hat{L}^{WAC}(\theta, \beta) \triangleq \frac{1}{n} \sum_{i=1}^n \hat{L}_i^{WAC}(\theta, \beta) \right\} \\ \hat{L}_i^{WAC}(\theta, \beta) \triangleq \beta_{[i]} \cdot \ell_{CE}(\theta; (\mathbf{x}_i, \mathbf{y}_i)) + (1 - \beta_{[i]}) \cdot \ell_{AC}(\theta; \mathbf{x}_i, A_{i,1}, A_{i,2}). \end{aligned} \quad (5)$$

With convex and continuous loss and regularization terms (formally in Proposition 1), Equation (5) admits a saddle point corresponding to  $\hat{\beta}$  which separates the label-sparse and label-dense samples under Assumption 1.

**Proposition 1** (Formal proof in Appendix A). Assume that  $\ell_{CE}(\theta; (\mathbf{x}, \mathbf{y}))$  and  $\ell_{AC}(\theta; \mathbf{x}, A_1, A_2)$  are convex and continuous in  $\theta$  for all  $(\mathbf{x}, \mathbf{y}) \in \mathcal{X} \times [K]^d$  and  $A_1, A_2 \sim \mathcal{A}^2$ ;  $\mathcal{F}_{\theta^*}(\gamma) \subset \mathcal{F}_\theta$  is compact and convex. If  $P_0$  and  $P_1$  are *n-separated* (Assumption 1), then there exists  $\hat{\beta} \in \{0, 1\}^n$  and  $\hat{\theta}^{WAC} \in \operatorname{argmin}_{\theta \in \mathcal{F}_{\theta^*}(\gamma)} \hat{L}^{WAC}(\theta, \hat{\beta})$  such that

$$\min_{\theta \in \mathcal{F}_{\theta^*}(\gamma)} \hat{L}^{WAC}(\theta, \hat{\beta}) = \hat{L}^{WAC}(\hat{\theta}^{WAC}, \hat{\beta}) = \max_{\beta \in [0,1]^n} \hat{L}^{WAC}(\hat{\theta}^{WAC}, \beta). \quad (6)$$

Further,  $\hat{\beta}$  separates the label-sparse and label-dense samples— $\hat{\beta}_{[i]} = \mathbb{I}\{(\mathbf{x}_i, \mathbf{y}_i) \sim P_1\}$ —w.h.p..

<sup>3</sup>We note that although Assumption 1 can be rather strong, it is only required for the separation guarantee of label-sparse and label-dense samples with high probability in Proposition 1, but not for the adaptive weighting algorithm introduced in Section 4 or in practice for the experiments.

<sup>4</sup>With pretrained initialization, we assume that the optimization algorithm is always probing in  $\mathcal{F}_{\theta^*}(\gamma)$ .

In other words, for  $n$  samples drawn from a mixture of  $n$ -separated  $P_0$  and  $P_1$ , the saddle point of  $L_i^{WAC}(\theta, \beta)$  in Equation (5) corresponds to  $\beta_{[i]} = 0$  on label-sparse samples (learning more from the unsupervised consistency regularization), and  $\beta_{[i]} = 1$  on label-dense samples (emphasizing the supervised averaged cross-entropy loss).

*Remark 2* (Connection to hard thresholding algorithms). At the saddle point of Equation (5),  $\min_{\theta \in \mathcal{F}_{\theta^*}(\gamma)} \hat{L}^{WAC}(\theta, \hat{\beta})$  is closely related to hard thresholding algorithms like Ordered SGD [Kawaguchi and Lu, 2020] and iterative trimmed loss [Shen and Sanghavi, 2019]. At each iteration, these algorithms update the model on a proper subset of supervised training samples based on the (ranking of) current empirical risks. Compared to hard thresholding algorithms, (i) Equation (5) additionally leverages unsupervised consistency regularization on the unused samples (e.g., label-sparse samples) for improving generalization; meanwhile, (ii) it does not require prior knowledge on the ratios of sample subpopulations (e.g.,  $\xi$  for  $P_\xi$ ) which is essential for hard thresholding algorithms. Equation (5) further facilitates the more flexible optimization process. As we will empirically show in Table 2, despite the close relation between Equation (5) and the hard thresholding algorithms (Remark 2), such updating strategies may be suboptimal for solving Equation (5).

## 4 Adaptively Weighted Augmentation Consistency (AdaWAC)

Inspired by the breakthrough made by Sagawa et al. [2020] in the distributionally-robust optimization (DRO) setting where gradient updating on weights is shown to enjoy better convergence guarantees than hard thresholding, we introduce an adaptive weighting algorithm for solving Equation (5) based on online mirror descent. Our algorithm is outlined in Algorithm 1. The flexibility of online mirror descent in choosing the associated norm space not only allows gradient updates on sample weights, but also grants distinct learning dynamics to sample weights  $\beta_t$  and model parameters  $\theta_t$ , which leads to the following convergence guarantee.

---

### Algorithm 1 Adaptively Weighted Augmentation Consistency (AdaWAC)

---

- 1: **Input:** Training samples  $\{(\mathbf{x}_i, \mathbf{y}_i)\}_{i \in [n]} \sim P_\xi^n$ , augmentations  $\{(A_{i,1}, A_{i,2})\}_{i \in [n]} \sim \mathcal{A}^{2n}$ , maximum number of iterations  $T \in \mathbb{N}$ , learning rates  $\eta_\theta, \eta_\beta > 0$ , pretrained initialization for the pixel-wise classifier  $\theta_0 \in \mathcal{F}_{\theta^*}(\gamma)$ .
  - 2: Initialize the sample weights  $\beta_0 = \mathbf{1}/2 \in [0, 1]^n$ .
  - 3: **for**  $t = 1, \dots, T$  **do**
  - 4:   Sample  $i_t \sim [n]$  uniformly
  - 5:    $\mathbf{b} \leftarrow [(\beta_{t-1})_{[i_t]}, 1 - (\beta_{t-1})_{[i_t]}]$
  - 6:    $\mathbf{b}_{[1]} \leftarrow \mathbf{b}_{[1]} \cdot \exp(\eta_\beta \cdot \ell_{CE}(\theta_{t-1}; (\mathbf{x}_{i_t}, \mathbf{y}_{i_t})))$
  - 7:    $\mathbf{b}_{[2]} \leftarrow \mathbf{b}_{[2]} \cdot \exp(\eta_\beta \cdot \ell_{AC}(\theta_{t-1}; \mathbf{x}_{i_t}, A_{i_t,1}, A_{i_t,2}))$
  - 8:    $\beta_t \leftarrow \beta_{t-1}, (\beta_t)_{[i_t]} \leftarrow \mathbf{b}_{[1]} / \|\mathbf{b}\|_1$
  - 9:    $\theta_t \leftarrow \theta_{t-1} - \eta_\theta \cdot \left( (\beta_t)_{[i_t]} \cdot \nabla_\theta \ell_{CE}(\theta_{t-1}; (\mathbf{x}_{i_t}, \mathbf{y}_{i_t})) \right. \\ \left. + (1 - (\beta_t)_{[i_t]}) \cdot \nabla_\theta \ell_{AC}(\theta_{t-1}; \mathbf{x}_{i_t}, A_{i_t,1}, A_{i_t,2}) \right)$
  - 10: **end for**
- 

**Proposition 2** (Formally in Proposition 3, proof in Appendix B, assumptions instantiated in Example 1). Assume that  $\ell_{CE}(\theta; (\mathbf{x}, \mathbf{y}))$  and  $\ell_{AC}(\theta; \mathbf{x}, A_1, A_2)$  are convex and continuous in  $\theta$  for all  $(\mathbf{x}, \mathbf{y}) \in \mathcal{X} \times [K]^d$  and  $A_1, A_2 \sim \mathcal{A}^2$ . Assume moreover that  $\mathcal{F}_{\theta^*}(\gamma) \subset \mathcal{F}_\theta$  is convex and compact. If there exist <sup>5</sup> (i)  $C_{\theta,*} > 0$  such that  $\frac{1}{n} \sum_{i=1}^n \left\| \nabla_\theta \hat{L}_i^{WAC}(\theta, \beta) \right\|_{\mathcal{F},*}^2 \leq C_{\theta,*}^2$  and (ii)  $C_{\beta,*} > 0$

<sup>5</sup>Following the convention, we use  $*$  in subscription to denote the dual spaces. For instance, recalling the parameter

such that  $\frac{1}{n} \sum_{i=1}^n \max \{ \ell_{CE}(\theta; (\mathbf{x}_i, \mathbf{y}_i)), \ell_{AC}(\theta; \mathbf{x}_i, A_{i,1}, A_{i,2}) \}^2 \leq C_{\beta,*}^2$  for all  $\theta \in \mathcal{F}_{\theta*}(\gamma)$ ,  $\beta \in [0, 1]^n$ , then with  $\eta_\theta = \eta_\beta = \frac{2}{\sqrt{5T(\gamma^2 C_{\theta,*}^2 + 2nC_{\beta,*}^2)}}$ , Algorithm 1 provides

$$\mathbb{E} \left[ \max_{\beta \in [0,1]^n} \widehat{L}^{WAC}(\bar{\theta}_T, \beta) - \min_{\theta \in \mathcal{F}_{\theta*}(\gamma)} \widehat{L}^{WAC}(\theta, \bar{\beta}_T) \right] \leq 2\sqrt{5(\gamma^2 C_{\theta,*}^2 + 2nC_{\beta,*}^2)} / T$$

where  $\bar{\theta}_T = \frac{1}{T} \sum_{t=1}^T \theta_t$  and  $\bar{\beta}_T = \frac{1}{T} \sum_{t=1}^T \beta_t$ .

In addition to the convergence guarantee, Algorithm 1 also demonstrates superior performance over hard thresholding algorithms for segmentation problems in practice (Table 2). An intuitive explanation is that instead of filtering out all the label-sparse samples via hard thresholding, the adaptive weighting allows the model to learn from some sparse labels at the early epochs, while smoothly down-weighting  $\ell_{CE}$  of these samples since learning sparse labels tends to be easier (Remark 1). With the learned model tested on a mixture of label-sparse and label-dense samples, learning sparse labels at the early stage is crucial for accurate segmentation.

## 5 Experiments

In this section, we compare the proposed *AdaWAC* (Algorithm 1) to some related algorithms based on empirical risk minimization/hard thresholding that achieve state-of-the-art performance on several benchmark medical image segmentation tasks. We first demonstrate the performance improvements brought by *AdaWAC* in terms of sample efficiency and robustness to subpopulation shift. Then, we compare *AdaWAC* to the closely related hard thresholding algorithms [Kawaguchi and Lu, 2020, Shen and Sanghavi, 2019] and verify its empirical advantage as suggested in Remark 2. Our ablation study further illustrates the indispensability of both the sample reweighting and consistency regularization, the careful combination of which leads to the superior performance of *AdaWAC*<sup>6</sup>.

**Experimental setup.** We conduct experiments on two volumetric medical image segmentation tasks: abdominal CT segmentation for Synapse multi-organ dataset (Synapse)<sup>7</sup> and cine-MRI segmentation for Automated cardiac diagnosis challenge dataset (ACDC)<sup>8</sup>. We follow the official implementation of TransUNet [Chen et al., 2021] for the baseline architecture and evaluate segmentations with two standard metrics—the average Dice-similarity coefficient (DSC) and average 95-percentile of Hausdorff distance (HD95). Dataset descriptions and implementation details are deferred to Appendix D. Given the sensitivity of medical image semantics to perturbations, our experiments only involve simple augmentations (*i.e.*, rotation and mirroring) adapted from [Chen et al., 2021].

It is worth to highlight that, in addition to the subpopulation shift between sparse and dense labels within each volume studied in this work, the pixel-wise class imbalance (*e.g.*, the predominance of background pixels within each image) is another well-investigated challenge for medical image segmentation, where coupling the dice loss [Taghanaki et al., 2019b, Wong et al., 2018, Yeung et al., 2022] in the objective is a common remedy used in many state-of-the-art methods [Cao et al., 2021, Chen et al., 2021]. The implementation of *AdaWAC* also leverages the dice loss to alleviate pixel-wise class imbalance. We defer the detailed discussion to Appendix C.

space  $\mathcal{F}_\theta$  characterized by the norm  $\|\cdot\|_{\mathcal{F}}$  from Section 2.1, we use  $\|\cdot\|_{\mathcal{F},*}$  to denote its dual norm; while  $C_{\theta,*}$ ,  $C_{\beta,*}$  upper bound the dual norms of the gradients with respect to  $\theta$  and  $\beta$ .

<sup>6</sup>The implementation of *AdaWAC* is released at <https://github.com/gail-yxie/adawac>.

<sup>7</sup><https://www.synapse.org/#!/Synapse:syn3193805/wiki/217789>

<sup>8</sup><https://www.creatis.insa-lyon.fr/Challenge/acdc/>

## 5.1 Segmentation Performance of *AdaWAC*

**Image Segmentation on Synapse.** Figure 2 visualizes the segmentation predictions given by the model trained with *AdaWAC* (ours) and the TransUNet [Chen et al., 2021] baseline on 6 ordered slices in one of the Synapse test volumes. We observe that the *AdaWAC* model provides more accurate predictions on the segmentation boundaries and captures small organs better than the baseline.

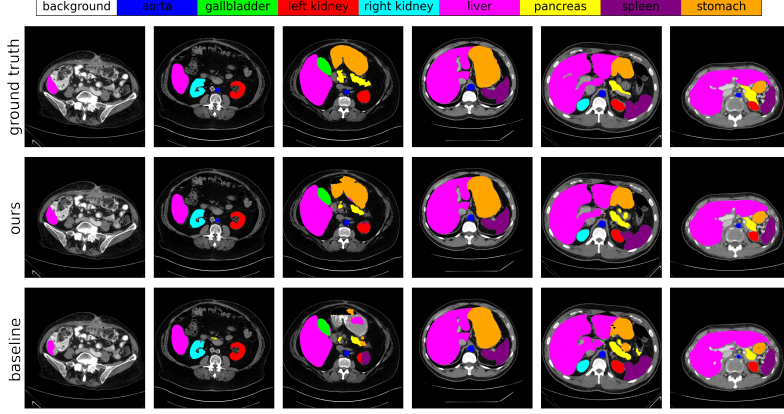


Figure 2: Visualization of segmentation predictions against the ground truth (in grayscale) on Synapse. Top to bottom: ground truth, ours (*AdaWAC*), baseline (TransUNet [Chen et al., 2021]).

**Visualization of *AdaWAC*.** As shown in Figure 3, with  $\ell_{CE}(\theta_t; (\mathbf{x}_i, \mathbf{y}_i))$  (Equation (2)) of label-sparse versus label-dense slices weakly separated in the early epochs, the model further learns to distinguish  $\ell_{CE}(\theta_t; (\mathbf{x}_i, \mathbf{y}_i))$  of label-sparse/label-dense slices during training. By contrast,  $\ell_{AC}(\theta_t; \mathbf{x}_i, A_{i,1}, A_{i,2})$  (Equation (3)) remains mixed for all slices throughout the entire training process. As a result, the CE weights of label-sparse slices are much smaller than those of label-dense ones, pushing *AdaWAC* to learn more image representations but fewer pixel classification for slices with sparse labels and learn more pixel classification for slices with dense labels.

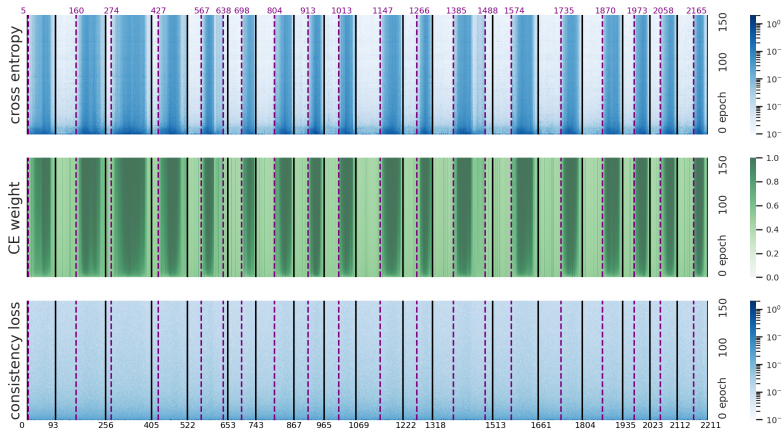


Figure 3:  $\ell_{CE}(\theta_t; (\mathbf{x}_i, \mathbf{y}_i))$  (top), CE weights  $\beta_t$  (middle), and  $\ell_{AC}(\theta_t; \mathbf{x}_i, A_{i,1}, A_{i,2})$  (bottom) of the entire Synapse training process. The x-axis indexes slices 0–2211. The y-axis enumerates epochs 0–150. Individual volumes (cases) are partitioned by black lines, while purple lines separate slices with/without non-background pixels.



**Sample efficiency and robustness.** We first demonstrate the *sample efficiency* of *AdaWAC* compared to the TransUNet baseline when training only on proper subsets of the entire Synapse training set (“full” in Table 1). Specifically, we consider the following training subsets: (i) **half-vol** consisting of 9 volumes uniformly sampled from the total 18 volumes in **full**, (ii) **half-slice** containing slices with even indices only in each volume<sup>9</sup>, (iii) **half-sparse** with the first half slices in each volume, most of which tend to be label-sparse (Figure 3). As shown in Table 1, the model trained with *AdaWAC* on **half-slice** generalizes as well as a baseline model trained on **full**, if not better. Moreover, the **half-sparse** experiments illustrate the *robustness* of *AdaWAC* under subpopulation shift where the baseline model collapses due to the dominance of sparse-labeled slices.

Table 1: *AdaWAC* versus TransUNet baseline on the full Synapse and its proper subsets.

Training	Method	DSC $\uparrow$	HD95 $\downarrow$	Aorta	Gallbladder	Kidney (L)	Kidney (R)	Liver	Pancreas	Spleen	Stomach
full	baseline	76.28	29.23	<b>87.46</b>	<b>55.21</b>	82.06	77.76	94.10	54.06	85.07	74.54
	<i>AdaWAC</i>	<b>79.12</b>	<b>25.79</b>	87.23	54.94	<b>84.58</b>	<b>81.69</b>	<b>94.62</b>	<b>58.29</b>	<b>90.63</b>	<b>81.01</b>
half-vol	baseline	71.61	35.86	83.29	35.37	78.25	<b>77.25</b>	92.92	51.32	83.80	70.66
	<i>AdaWAC</i>	<b>74.89</b>	<b>34.95</b>	<b>84.45</b>	<b>52.07</b>	<b>79.59</b>	6.06	<b>93.19</b>	<b>54.46</b>	<b>84.91</b>	<b>74.37</b>
half-slice	baseline	75.19	<b>24.66</b>	86.26	49.28	79.32	76.55	94.34	54.04	<b>86.20</b>	75.57
	<i>AdaWAC</i>	<b>77.09</b>	29.75	<b>86.66</b>	<b>53.95</b>	<b>81.36</b>	<b>78.84</b>	<b>94.60</b>	<b>57.95</b>	85.38	<b>78.01</b>
half-sparse	baseline	1.04	0.00	0.00	8.33	0.00	0.00	0.00	0.00	0.00	0.00
	<i>AdaWAC</i>	<b>40.72</b>	<b>80.93</b>	<b>76.59</b>	<b>8.33</b>	<b>66.53</b>	<b>62.11</b>	<b>49.69</b>	<b>31.09</b>	<b>12.30</b>	<b>19.11</b>

**Comparison with hard thresholding algorithms.** Table 2 illustrates the empirical advantage of *AdaWAC* over the hard thresholding algorithms [Kawaguchi and Lu, 2020, Shen and Sanghavi, 2019], as suggested in Remark 2, on volumetric medical image segmentation tasks like Synapse. In Table 2, (i) **trim-train** learns only from slices with at least one non-background pixel and trims the rest in each iteration on the fly; (ii) **trim-ratio** ranks the cross-entropy loss  $\ell_{CE}(\theta_t; (\mathbf{x}_i, \mathbf{y}_i))$  in each iteration (mini-batch) and trims samples with the lowest cross-entropy losses at a fixed ratio – the ratio of all-background slices in the full training set ( $1 - \frac{1280}{2211} \approx 0.42$ ), updating only those samples with the larger cross-entropy losses; (iii) **ACR** further incorporates the augmentation consistency regularization directly via addition of  $\ell_{AC}(\theta_t; \mathbf{x}_i, A_{i,1}, A_{i,2})$  without reweighting. We notice that naive incorporation of **ACR** fail to bring observable boosts to the hard-thresholding methods. Therefore, the deliberate combination via reweighting in *AdaWAC* is essential for performance improvement.

Table 2: *AdaWAC* versus hard thresholding algorithms on Synapse.

Method	baseline	trim-train		trim-ratio		<i>AdaWAC</i>
		+ACR		+ACR		
DSC $\uparrow$	76.28	76.01	75.66	74.26	77.98	<b>79.12</b>
HD95 $\downarrow$	29.23	26.94	35.06	28.59	33.59	<b>25.79</b>

**Image Segmentation on ACDC.** Performance improvements granted by *AdaWAC* are also observed on the ACDC dataset (Table 3). We defer detailed visualization of ACDC segmentation to Appendix E.

<sup>9</sup>Such sampling is equivalent to doubling the time interval between two consecutive scans or halving the scanning frequency in practice, resulting in the halving of sample size.

Table 3: *AdaWAC* versus TransUNet baseline on ACDC.

Method	DSC $\uparrow$	HD95 $\downarrow$	RV	Myo	LV
TransUNet	89.36	3.02	88.36	83.84	95.87
<i>AdaWAC</i> (ours)	<b>90.41</b>	<b>1.29</b>	<b>89.50</b>	<b>85.78</b>	<b>95.95</b>

## 5.2 Ablation Study

Table 4: The roles of sample reweighting and consistency regularization in *AdaWAC* on Synapse.

Method	DSC $\uparrow$	HD95 $\downarrow$	Aorta	Gallbladder	Kidney (L)	Kidney (R)	Liver	Pancreas	Spleen	Stomach
baseline	76.28	29.23	87.46	<b>55.21</b>	82.06	77.76	94.10	54.06	85.07	74.54
reweight-only	76.68	29.24	86.15	53.98	82.96	80.28	93.42	55.86	85.29	75.49
ACR-only	77.89	31.65	<b>87.96</b>	54.34	81.79	80.21	94.52	<b>60.41</b>	88.07	75.83
<i>AdaWAC</i> -0.01	77.94	27.81	87.58	52.75	82.29	80.22	<b>94.90</b>	55.92	<b>91.63</b>	78.23
<i>AdaWAC</i> -1.0	<b>79.12</b>	<b>25.79</b>	87.23	54.94	<b>84.58</b>	<b>81.69</b>	94.62	58.29	90.63	<b>81.01</b>

**On the influence of consistency regularization.** To illustrate the role of data augmentation consistency regularization in *AdaWAC*, we consider the **reweight-only** scenario with  $\lambda_{AC} = 0$  such that  $\ell_{AC}(\theta_t; \mathbf{x}_i, A_{i,1}, A_{i,2}) \equiv 0$  and therefore  $\mathbf{b}_{[2]}$  (Algorithm 1 line 7) remains intact. By setting consistency regularization in *AdaWAC* to zero, reweighting alone brings little improvement compared to the baseline (Table 4).

**On the influence of sample reweighting.** We now investigate the effect of sample reweighting under different reweighting learning rates  $\eta_\beta$  (recall Algorithm 1): (i) **ACR-only** for  $\eta_\beta = 0$  (equivalent to the naive addition of  $\ell_{AC}(\theta_t; \mathbf{x}_i, A_{i,1}, A_{i,2})$ ), (ii) ***AdaWAC*-0.01** for  $\eta_\beta = 0.01$ , and (iii) ***AdaWAC*-1.0** for  $\eta_\beta = 1.0$ . As Table 4 implies, when removing reweighting from *AdaWAC*, augmentation consistency regularization alone improves DSC slightly from 76.28 (baseline) to 77.89 (ACR-only), whereas *AdaWAC* boosts DSC to 79.12 (*AdaWAC*-1.0) with a proper choice of  $\eta_\beta$ .

## 6 Discussion

In this paper, we exploit the non-uniformity in labels commonly observed in volumetric medical image segmentation via a new algorithm *AdaWAC*, which can be viewed as a careful combination of adaptive weighting and augmentation consistency regularization. By casting the separation between sparse and dense segmentation labels as a subpopulation shift in the label distribution, we leverage the unsupervised consistency regularization on encoder layer outputs (of UNet architectures) as a natural reference for distinguishing label-sparse and label-dense samples via comparisons against the supervised average cross-entropy loss. We formulate such comparisons as a weighted augmentation consistency (WAC) regularization problem and propose an adaptive weighting scheme—*AdaWAC*—for iterative and smooth separation of samples from different subpopulations with a convergence guarantee. Our experiments demonstrate empirical effectiveness of *AdaWAC* not only in improving segmentation performance and sample efficiency but also in enhancing robustness to the subpopulation shift in labels.

**Acknowledgement.** R. Ward was partially supported by AFOSR MURI FA9550-19-1-0005, NSF DMS 1952735, NSF HDR1934932, and NSF 2019844. Y. Dong was supported by NSF

DMS 1952735. Y. Xie was supported by NSF 2019844. The authors wish to thank Qi Lei and Xiaoxia Wu for valuable discussions and Jieneng Chen for generously providing preprocessed medical image segmentation datasets.

## References

- G. Alain, A. Lamb, C. Sankar, A. Courville, and Y. Bengio. Variance reduction in sgd by distributed importance sampling. *arXiv preprint arXiv:1511.06481*, 2015.
- P. Bachman, O. Alsharif, and D. Precup. Learning with pseudo-ensembles. *Advances in neural information processing systems*, 27:3365–3373, 2014.
- H. Basak, R. Bhattacharya, R. Hussain, and A. Chatterjee. An embarrassingly simple consistency regularization method for semi-supervised medical image segmentation. *arXiv preprint arXiv:2202.00677*, 2022.
- A. Ben-Tal, D. den Hertog, A. D. Waegenaere, B. Melenberg, and G. Rennen. Robust solutions of optimization problems affected by uncertain probabilities. *Management Science*, 59(2):341–357, 2013. ISSN 00251909, 15265501.
- D. Bertsekas. *Convex optimization theory*, volume 1. Athena Scientific, 2009.
- G. Bortsova, F. Dubost, L. Hogeweg, I. Katramados, and M. d. Bruijne. Semi-supervised medical image segmentation via learning consistency under transformations. In *International Conference on Medical Image Computing and Computer-Assisted Intervention*, pages 810–818. Springer, 2019.
- H. Cao, Y. Wang, J. Chen, D. Jiang, X. Zhang, Q. Tian, and M. Wang. Swin-unet: Unet-like pure transformer for medical image segmentation. *arXiv preprint arXiv:2105.05537*, 2021.
- J. Chen, Y. Lu, Q. Yu, X. Luo, E. Adeli, Y. Wang, L. Lu, A. L. Yuille, and Y. Zhou. Transunet: Transformers make strong encoders for medical image segmentation. *arXiv preprint arXiv:2102.04306*, 2021.
- J. Duchi and H. Namkoong. Learning models with uniform performance via distributionally robust optimization. *arXiv preprint arXiv:1810.08750*, 2018.
- J. Duchi, P. Glynn, and H. Namkoong. Statistics of robust optimization: A generalized empirical likelihood approach. *arXiv preprint arXiv:1610.03425*, 2016.
- S. Gopal. Adaptive sampling for sgd by exploiting side information. In *Proceedings of the 33rd International Conference on International Conference on Machine Learning - Volume 48*, ICML’16, page 364–372. JMLR.org, 2016.
- G. Hachohen and D. Weinshall. On the power of curriculum learning in training deep networks. In *International Conference on Machine Learning*, pages 2535–2544. PMLR, 2019.
- J. Haddock, D. Needell, E. Rebrova, and W. Swartworth. Quantile-based Iterative Methods for Corrupted Systems of Linear Equations. *arXiv:2009.08089 [cs, math]*, Sept. 2020. arXiv: 2009.08089.
- A. Katharopoulos and F. Fleuret. Not all samples are created equal: Deep learning with importance sampling. In *International conference on machine learning*, pages 2525–2534. PMLR, 2018.

- K. Kawaguchi and H. Lu. Ordered sgd: A new stochastic optimization framework for empirical risk minimization. In *International Conference on Artificial Intelligence and Statistics*, pages 669–679. PMLR, 2020.
- S. Laine and T. Aila. Temporal ensembling for semi-supervised learning. *arXiv preprint arXiv:1610.02242*, 2016.
- X. Li, L. Yu, H. Chen, C.-W. Fu, L. Xing, and P.-A. Heng. Transformation-consistent self-ensembling model for semisupervised medical image segmentation. *IEEE Transactions on Neural Networks and Learning Systems*, 32(2):523–534, 2020.
- I. Loshchilov and F. Hutter. Online batch selection for faster training of neural networks. *arXiv preprint arXiv:1511.06343*, 2015.
- F. Milletari, N. Navab, and S.-A. Ahmadi. V-net: Fully convolutional neural networks for volumetric medical image segmentation. In *2016 Fourth International Conference on 3D Vision (3DV)*, pages 565–571, 2016.
- D. Needell, R. Ward, and N. Srebro. Stochastic gradient descent, weighted sampling, and the randomized kaczmarz algorithm. *Advances in neural information processing systems*, 27, 2014.
- A. Nemirovski, A. Juditsky, G. Lan, and A. Shapiro. Robust stochastic approximation approach to stochastic programming. *SIAM Journal on Optimization*, 19(4):1574–1609, 2009.
- S. J. Russell and P. Norvig. Artificial intelligence: a modern approach. malaysia, 2016.
- S. Sagawa, P. W. Koh, T. B. Hashimoto, and P. Liang. Distributionally robust neural networks. In *International Conference on Learning Representations*, 2020.
- V. Shah, X. Wu, and S. Sanghavi. Choosing the sample with lowest loss makes sgd robust. In *Proceedings of the Twenty Third International Conference on Artificial Intelligence and Statistics*, volume 108 of *Proceedings of Machine Learning Research*, pages 2120–2130, Online, 26–28 Aug 2020. PMLR.
- Y. Shen and S. Sanghavi. Learning with bad training data via iterative trimmed loss minimization. In *International Conference on Machine Learning*, pages 5739–5748. PMLR, 2019.
- M. Sion. On general minimax theorems. *Pacific Journal of Mathematics*, 8(1):171 – 176, 1958.
- K. Sohn, D. Berthelot, N. Carlini, Z. Zhang, H. Zhang, C. A. Raffel, E. D. Cubuk, A. Kurakin, and C.-L. Li. Fixmatch: Simplifying semi-supervised learning with consistency and confidence. *Advances in neural information processing systems*, 33:596–608, 2020.
- S. A. Taghanaki, K. Abhishek, J. P. Cohen, J. Cohen-Adad, and G. Hamarneh. Deep semantic segmentation of natural and medical images: A review, 2019a.
- S. A. Taghanaki, Y. Zheng, S. K. Zhou, B. Georgescu, P. Sharma, D. Xu, D. Comaniciu, and G. Hamarneh. Combo loss: Handling input and output imbalance in multi-organ segmentation. *Computerized Medical Imaging and Graphics*, 75:24–33, 2019b.
- Y. Tang, X. Wang, A. P. Harrison, L. Lu, J. Xiao, and R. M. Summers. Attention-guided curriculum learning for weakly supervised classification and localization of thoracic diseases on chest radiographs. In *International Workshop on Machine Learning in Medical Imaging*, pages 249–258. Springer, 2018.

- J. G. Tullis and A. S. Benjamin. On the effectiveness of self-paced learning. *Journal of memory and language*, 64(2):109–118, 2011.
- X. Wang, H. Chen, H. Xiang, H. Lin, X. Lin, and P.-A. Heng. Deep virtual adversarial self-training with consistency regularization for semi-supervised medical image classification. *Medical image analysis*, 70:102010, 2021a.
- X. Wang, Y. Chen, and W. Zhu. A survey on curriculum learning. *IEEE Transactions on Pattern Analysis and Machine Intelligence*, 2021b.
- Y. Wang, W. Liu, X. Ma, J. Bailey, H. Zha, L. Song, and S.-T. Xia. Iterative Learning with Open-set Noisy Labels. *arXiv:1804.00092 [cs]*, Mar. 2018. arXiv: 1804.00092.
- K. C. L. Wong, M. Moradi, H. Tang, and T. Syeda-Mahmood. 3d segmentation with exponential logarithmic loss for highly unbalanced object sizes. In A. F. Frangi, J. A. Schnabel, C. Davatzikos, C. Alberola-López, and G. Fichtinger, editors, *Medical Image Computing and Computer Assisted Intervention – MICCAI 2018*, pages 612–619, Cham, 2018. Springer International Publishing. ISBN 978-3-030-00931-1.
- X. Wu, Y. Xie, S. S. Du, and R. Ward. Adaloss: A computationally-efficient and provably convergent adaptive gradient method. *Proceedings of the AAAI Conference on Artificial Intelligence*, 36(8):8691–8699, Jun. 2022.
- M. Yeung, E. Sala, C.-B. Schönlieb, and L. Rundo. Unified focal loss: Generalising dice and cross entropy-based losses to handle class imbalanced medical image segmentation. *Computerized Medical Imaging and Graphics*, 95:102026, 2022. ISSN 0895-6111.
- H. Zhang, M. Cisse, Y. N. Dauphin, and D. Lopez-Paz. mixup: Beyond empirical risk minimization. *arXiv preprint arXiv:1710.09412*, 2017.
- Y. Zhang, B. Zhou, L. Chen, Y. Wu, and H. Zhou. Multi-transformation consistency regularization for semi-supervised medical image segmentation. In *2021 4th International Conference on Artificial Intelligence and Big Data (ICAIBD)*, pages 485–489. IEEE, 2021.
- A. Zhao, G. Balakrishnan, F. Durand, J. V. Guttag, and A. V. Dalca. Data augmentation using learned transformations for one-shot medical image segmentation. In *Proceedings of the IEEE/CVF conference on computer vision and pattern recognition*, pages 8543–8553, 2019.
- P. Zhao and T. Zhang. Stochastic optimization with importance sampling for regularized loss minimization. In *international conference on machine learning*, pages 1–9. PMLR, 2015.
- H.-Y. Zhou, C. Wang, H. Li, G. Wang, S. Zhang, W. Li, and Y. Yu. Ssmc: semi-supervised medical image detection with adaptive consistency and heterogeneous perturbation. *Medical Image Analysis*, 72:102117, 2021.



## A Separation of Label-sparse and Label-dense Samples

*Proof of Proposition 1.* We first observe that, since  $\ell_{CE}(\theta; (\mathbf{x}, \mathbf{y}))$  and  $\ell_{AC}(\theta; \mathbf{x}, A_1, A_2)$  are convex and continuous in  $\theta$  for all  $(\mathbf{x}, \mathbf{y}) \in \mathcal{X} \times \mathcal{Y}$  and  $A_1, A_2 \sim \mathcal{A}^2$ , for all  $i \in [n]$ ,  $\hat{L}_i^{WAC}(\theta, \beta)$  is continuous, convex in  $\theta$ , and affine (thus concave) in  $\beta$ ; and therefore so is  $\hat{L}^{WAC}(\theta, \beta)$ . Then with the compact and convex domains  $\theta \in \mathcal{F}_{\theta^*}(\gamma)$  and  $\beta \in [0, 1]^n$ , Sion's minimax theorem [Sion, 1958] suggests the minimax equality,

$$\min_{\theta \in \mathcal{F}_{\theta^*}(\gamma)} \max_{\beta \in [0, 1]^n} \hat{L}^{WAC}(\theta, \beta) = \max_{\beta \in [0, 1]^n} \min_{\theta \in \mathcal{F}_{\theta^*}(\gamma)} \hat{L}^{WAC}(\theta, \beta), \quad (7)$$

where inf, sup can be replaced by min, max respectively due to compactness of the domains.

Further, by the continuity and convexity-concavity of  $\hat{L}^{WAC}(\theta, \beta)$ , the pointwise maximum  $\max_{\beta \in [0, 1]^n} \hat{L}^{WAC}(\theta, \beta)$  is lower semi-continuous and convex in  $\theta$  while the pointwise minimum  $\min_{\theta \in \mathcal{F}_{\theta^*}(\gamma)} \hat{L}^{WAC}(\theta, \beta)$  is upper semi-continuous and concave in  $\beta$ . Then via Weierstrass' theorem (Bertsekas [2009], Proposition 3.2.1), there exist  $\hat{\theta}^{WAC} \in \mathcal{F}_{\theta^*}(\gamma)$  and  $\hat{\beta} \in [0, 1]^n$  that achieve the minimax optimal by minimizing  $\max_{\beta \in [0, 1]^n} \hat{L}^{WAC}(\theta, \beta)$  and maximizing  $\min_{\theta \in \mathcal{F}_{\theta^*}(\gamma)} \hat{L}^{WAC}(\theta, \beta)$ . Along with Equation (7), such  $(\hat{\theta}^{WAC}, \hat{\beta})$  provides a saddle point for Equation (5) (Bertsekas [2009], Proposition 3.4.1).

Next, we show via contradiction that there exists a saddle point with  $\hat{\beta}$  attained on a vertex  $\hat{\beta} \in \{0, 1\}^n$ . Suppose the opposite, then for any saddle point  $(\hat{\theta}^{WAC}, \hat{\beta})$ , there must be an  $i \in [n]$  with  $\hat{\beta}_{[i]} \in (0, 1)$ , where we have the following contradictions:

- (i) If  $\ell_{CE}(\hat{\theta}^{WAC}; (\mathbf{x}_i, \mathbf{y}_i)) < \ell_{AC}(\hat{\theta}^{WAC}; \mathbf{x}_i, A_{i,1}, A_{i,2})$ , decreasing  $\hat{\beta}_{[i]} > 0$  to  $\hat{\beta}'_{[i]} = 0$  leads to  $\hat{L}^{WAC}(\hat{\theta}^{WAC}, \hat{\beta}') > \hat{L}^{WAC}(\hat{\theta}^{WAC}, \hat{\beta})$ , contradicting Equation (6).
- (ii) If  $\ell_{CE}(\hat{\theta}^{WAC}; (\mathbf{x}_i, \mathbf{y}_i)) > \ell_{AC}(\hat{\theta}^{WAC}; \mathbf{x}_i, A_{i,1}, A_{i,2})$ , increasing  $\hat{\beta}_{[i]} < 1$  to  $\hat{\beta}'_{[i]} = 1$  again leads to  $\hat{L}^{WAC}(\hat{\theta}^{WAC}, \hat{\beta}') > \hat{L}^{WAC}(\hat{\theta}^{WAC}, \hat{\beta})$ , contradicting Equation (6).
- (iii) If  $\ell_{CE}(\hat{\theta}^{WAC}; (\mathbf{x}_i, \mathbf{y}_i)) = \ell_{AC}(\hat{\theta}^{WAC}; \mathbf{x}_i, A_{i,1}, A_{i,2})$ ,  $\hat{\beta}_{[i]}$  can be replaced with any value in  $[0, 1]$ , including 0, 1.

Therefore, there must be a saddle point  $(\hat{\theta}^{WAC}, \hat{\beta})$  with  $\hat{\beta} \in \{0, 1\}^n$  such that

$$\beta_{[i]} = \mathbb{I} \left\{ \ell_{CE}(\hat{\theta}^{WAC}; (\mathbf{x}_i, \mathbf{y}_i)) > \ell_{AC}(\hat{\theta}^{WAC}; \mathbf{x}_i, A_{i,1}, A_{i,2}) \right\}.$$

Finally, it remains to show that *w.h.p.* over  $\{(\mathbf{x}_i, \mathbf{y}_i)\}_{i \in [n]} \sim P_\xi^n$  and  $\{(A_{i,1}, A_{i,2})\}_{i \in [n]} \sim \mathcal{A}^{2n}$ ,

- (i)  $\ell_{CE}(\hat{\theta}^{WAC}; (\mathbf{x}_i, \mathbf{y}_i)) \leq \ell_{AC}(\hat{\theta}^{WAC}; \mathbf{x}_i, A_{i,1}, A_{i,2})$  for all  $(\mathbf{x}_i, \mathbf{y}_i) \sim P_0$ ; and
- (ii)  $\ell_{CE}(\hat{\theta}^{WAC}; (\mathbf{x}_i, \mathbf{y}_i)) > \ell_{AC}(\hat{\theta}^{WAC}; \mathbf{x}_i, A_{i,1}, A_{i,2})$  for all  $(\mathbf{x}_i, \mathbf{y}_i) \sim P_1$ ;

which leads to  $\beta_{[i]} = \mathbb{I} \{ (\mathbf{x}_i, \mathbf{y}_i) \sim P_1 \}$  *w.h.p.* as desired. To illustrate this, we begin by observing that when  $P_0$  and  $P_1$  are  $n$ -separated (Assumption 1), since  $\hat{\theta}^{WAC} \in \mathcal{F}_{\theta^*}(\gamma)$ , there exists some  $\omega > 0$  such that for each  $i \in [n]$ ,

$$\mathbb{P} \left[ \ell_{CE}(\hat{\theta}^{WAC}; (\mathbf{x}_i, \mathbf{y}_i)) < \ell_{AC}(\hat{\theta}^{WAC}; \mathbf{x}_i, A_{i,1}, A_{i,2}) \mid (\mathbf{x}_i, \mathbf{y}_i) \sim P_0 \right] \geq 1 - \frac{1}{\Omega(n^{1+\omega})},$$

and

$$\mathbb{P} \left[ \ell_{CE}(\hat{\theta}^{WAC}; (\mathbf{x}_i, \mathbf{y}_i)) > \ell_{AC}(\hat{\theta}^{WAC}; \mathbf{x}_i, A_{i,1}, A_{i,2}) \mid (\mathbf{x}_i, \mathbf{y}_i) \sim P_1 \right] \geq 1 - \frac{1}{\Omega(n^{1+\omega})}.$$

Therefore by the union bound over the set of  $n$  samples  $\{(\mathbf{x}_i, \mathbf{y}_i)\}_{i \in [n]} \sim P_\xi^n$ ,

$$\mathbb{P} \left[ \ell_{CE} \left( \hat{\theta}^{\text{WAC}}; (\mathbf{x}_i, \mathbf{y}_i) \right) < \ell_{AC} \left( \hat{\theta}^{\text{WAC}}; \mathbf{x}_i, A_{i,1}, A_{i,2} \right) \forall (\mathbf{x}_i, \mathbf{y}_i) \sim P_0 \right] \geq 1 - \frac{1}{\Omega(n^\omega)}, \quad (8)$$

and

$$\mathbb{P} \left[ \ell_{CE} \left( \hat{\theta}^{\text{WAC}}; (\mathbf{x}_i, \mathbf{y}_i) \right) > \ell_{AC} \left( \hat{\theta}^{\text{WAC}}; \mathbf{x}_i, A_{i,1}, A_{i,2} \right) \forall (\mathbf{x}_i, \mathbf{y}_i) \sim P_1 \right] \geq 1 - \frac{1}{\Omega(n^\omega)}. \quad (9)$$

Applying the union bound again on Equation (8) and Equation (9), we have the desired condition holds with probability  $1 - \Omega(n^\omega)^{-1}$ , i.e., w.h.p..  $\square$

## B Convergence of AdaWAC

Recall the underlying function class  $\mathcal{F} \ni f_\theta$  parameterized by some  $\theta \in \mathcal{F}_\theta$  that we aim to learn for the pixel-wise classifier  $h_\theta = \operatorname{argmax}_{k \in [K]} f_\theta(\mathbf{x})_{[j,:]}, j \in [d]$ :

$$\mathcal{F} = \left\{ f_\theta = \phi_\theta \circ \psi_\theta \mid \phi_\theta : \mathcal{X} \rightarrow \mathcal{Z}, \psi_\theta : \mathcal{Z} \rightarrow [0, 1]^{d \times K} \right\}, \quad (10)$$

where  $\phi_\theta, \psi_\theta$  correspond to the encoder and decoder functions. Formally, we consider an inner product space of parameters  $(\mathcal{F}_\theta, \langle \cdot, \cdot \rangle_{\mathcal{F}})$  with the induced norm  $\|\cdot\|_{\mathcal{F}}$  and dual norm  $\|\cdot\|_{\mathcal{F},*}$ .

For any  $d \in \mathbb{N}$ , let  $\Delta_d^n \triangleq \{[\beta_1; \dots; \beta_n] \in [0, 1]^{n \times d} \mid \|\beta_i\|_1 = 1 \forall i \in [n]\}$ . Then Equation (5) can be reformulated as:

$$\begin{aligned} \hat{\theta}^{\text{WAC}}, \hat{\mathbf{B}} &= \operatorname{argmin}_{\theta \in \mathcal{F}_{\theta^*}(\gamma)} \operatorname{argmax}_{\mathbf{B} \in \Delta_2^n} \left\{ \hat{L}^{\text{WAC}}(\theta, \mathbf{B}) \triangleq \frac{1}{n} \sum_{i=1}^n \hat{L}_i^{\text{WAC}}(\theta, \mathbf{B}) \right\}, \\ \hat{L}_i^{\text{WAC}}(\theta, \mathbf{B}) &\triangleq \mathbf{B}_{[i,1]} \cdot \ell_{CE}(\theta; (\mathbf{x}_i, \mathbf{y}_i)) + \mathbf{B}_{[i,2]} \cdot \ell_{AC}(\theta; \mathbf{x}_i, A_{i,1}, A_{i,2}). \end{aligned} \quad (11)$$

**Proposition 3** (Convergence (formal restatement of Proposition 2)). *Assume that  $\ell_{CE}(\theta; (\mathbf{x}, \mathbf{y}))$  and  $\ell_{AC}(\theta; \mathbf{x}, A_1, A_2)$  are convex and continuous in  $\theta$  for all  $(\mathbf{x}, \mathbf{y}) \in \mathcal{X} \times \mathcal{Y}$  and  $A_1, A_2 \sim \mathcal{A}^2$ , and that  $\mathcal{F}_{\theta^*}(\gamma) \subset \mathcal{F}_\theta$  is convex and compact. If there exist*

- (i)  $C_{\theta,*} > 0$  such that  $\frac{1}{n} \sum_{i=1}^n \left\| \nabla_\theta \hat{L}_i^{\text{WAC}}(\theta, \mathbf{B}) \right\|_{\mathcal{F},*}^2 \leq C_{\theta,*}^2$  for all  $\theta \in \mathcal{F}_{\theta^*}(\gamma), \mathbf{B} \in \Delta_2^n$  and
- (ii)  $C_{\mathbf{B},*} > 0$  such that  $\frac{1}{n} \sum_{i=1}^n \max \{ \ell_{CE}(\theta; (\mathbf{x}_i, \mathbf{y}_i)), \ell_{AC}(\theta; \mathbf{x}_i, A_{i,1}, A_{i,2}) \}^2 \leq C_{\mathbf{B},*}^2$  for all  $\theta \in \mathcal{F}_{\theta^*}(\gamma)$ ,

then with  $\eta_\theta = \eta_{\mathbf{B}} = 2 / \sqrt{5T (\gamma^2 C_{\theta,*}^2 + 2n C_{\mathbf{B},*}^2)}$ , Algorithm 1 provides the convergence guarantee for the duality gap  $\mathcal{E}(\bar{\theta}_T, \bar{\mathbf{B}}_T) \triangleq \max_{\mathbf{B} \in \Delta_2^n} \hat{L}^{\text{WAC}}(\bar{\theta}_T, \mathbf{B}) - \min_{\theta \in \mathcal{F}_{\theta^*}(\gamma)} \hat{L}^{\text{WAC}}(\theta, \bar{\mathbf{B}}_T)$ :

$$\mathbb{E} [\mathcal{E}(\bar{\theta}_T, \bar{\mathbf{B}}_T)] \leq 2 \sqrt{\frac{5 (\gamma^2 C_{\theta,*}^2 + 2n C_{\mathbf{B},*}^2)}{T}},$$

where  $\bar{\theta}_T = \frac{1}{T} \sum_{t=1}^T \theta_t$  and  $\bar{\mathbf{B}}_T = \frac{1}{T} \sum_{t=1}^T \mathbf{B}_t$ .

*Proof of Proposition 3.* The proof is an application of the standard convergence guarantee for the online mirror descent on saddle point problems, as recapitulated in Lemma 1.

Specifically, for  $\mathbf{B} \in \Delta_2^n$ , we use the norm  $\|\mathbf{B}\|_{1,2} \triangleq \sqrt{\sum_{i=1}^n \left( \sum_{j=1}^2 |\mathbf{B}_{[i,j]}| \right)^2}$  with its dual norm  $\|\mathbf{B}\|_{1,2,*} \triangleq \sqrt{\sum_{i=1}^n (\max_{j \in [2]} |\mathbf{B}_{[i,j]}|)^2}$ . We consider a mirror map  $\varphi_{\mathbf{B}} : [0, 1]^{n \times 2} \rightarrow \mathbb{R}$

such that  $\varphi_{\mathbf{B}}(\mathbf{B}) = \sum_{i=1}^n \sum_{j=1}^2 \mathbf{B}_{[i,j]} \log \mathbf{B}_{[i,j]}$ . We observe that, since  $\mathbf{B}_{[i,\cdot]}, \mathbf{B}'_{[i,\cdot]} \in \Delta_2$  for all  $i \in [n]$ ,

$$D_{\varphi_{\mathbf{B}}}(\mathbf{B}, \mathbf{B}') = \sum_{i=1}^n \sum_{j=1}^2 \mathbf{B}_{[i,j]} \log \frac{\mathbf{B}_{[i,j]}}{\mathbf{B}'_{[i,j]}} \geq \frac{1}{2} \sum_{i=1}^n \left( \sum_{j=1}^2 |\mathbf{B}_{[i,j]} - \mathbf{B}'_{[i,j]}| \right)^2 = \frac{1}{2} \|\mathbf{B} - \mathbf{B}'\|_{1,2}^2,$$

and therefore  $\varphi_{\mathbf{B}}$  is 1-strongly convex with respect to  $\|\cdot\|_{1,2}$ . With such  $\varphi_{\mathbf{B}}$ , we have the associated Fenchel dual  $\varphi_{\mathbf{B}}^*(\mathbf{G}) = \sum_{i=1}^n \log \left( \sum_{j=1}^2 \exp(\mathbf{G}_{[i,j]}) \right)$ , along with the gradients

$$\nabla \varphi_{\mathbf{B}}(\mathbf{B})_{[i,j]} = 1 + \log \mathbf{B}_{[i,j]}, \quad \nabla \varphi_{\mathbf{B}}^*(\mathbf{G})_{[i,j]} = \frac{\exp(\mathbf{G}_{[i,j]})}{\sum_{j=1}^2 \exp(\mathbf{G}_{[i,j]})},$$

such that the mirror descent update on  $\mathbf{B}$  is given by

$$\begin{aligned} (\mathbf{B}_{t+1})_{[i,j]} &= \nabla \varphi_{\mathbf{B}}^* \left( \nabla \varphi_{\mathbf{B}}(\mathbf{B}_t) - \eta_{\mathbf{B}} \cdot \nabla_{\mathbf{B}} \widehat{L}_{i_t}^{\text{WAC}}(\theta_t, \mathbf{B}_t) \right) \\ &= \frac{(\mathbf{B}_t)_{[i,j]} \exp \left( \eta_{\mathbf{B}} \cdot \left( \nabla_{\mathbf{B}} \widehat{L}_{i_t}^{\text{WAC}}(\theta_t, \mathbf{B}_t) \right)_{[i,j]} \right)}{\sum_{j=1}^2 (\mathbf{B}_t)_{[i,j]} \exp \left( \eta_{\mathbf{B}} \cdot \left( \nabla_{\mathbf{B}} \widehat{L}_{i_t}^{\text{WAC}}(\theta_t, \mathbf{B}_t) \right)_{[i,j]} \right)}. \end{aligned}$$

For  $i_t \sim [n]$  uniformly, the stochastic gradient with respect to  $\mathbf{B}$  satisfies

$$\begin{aligned} &\mathbb{E}_{i_t \sim [n]} \left[ \left\| \nabla_{\mathbf{B}} \widehat{L}_{i_t}^{\text{WAC}}(\theta_t, \mathbf{B}_t) \right\|_{1,2,*}^2 \right] \\ &= \frac{1}{n} \sum_{i_t=1}^n \max \{ \ell_{CE}(\theta_t; (\mathbf{x}_{i_t}, \mathbf{y}_{i_t})), \ell_{AC}(\theta_t; \mathbf{x}_{i_t}, A_{i_t,1}, A_{i_t,2}) \}^2 \leq C_{\mathbf{B},*}^2. \end{aligned}$$

Further, in the distance induced by  $\varphi_{\mathbf{B}}$ , we have

$$R_{\Delta_2^n}^2 \triangleq \max_{\mathbf{B} \in \Delta_2^n} \varphi_{\mathbf{B}}(\mathbf{B}) - \min_{\mathbf{B} \in \Delta_2^n} \varphi_{\mathbf{B}}(\mathbf{B}) = 0 - \sum_{i=1}^n \sum_{j=1}^2 \frac{1}{2} \log \frac{1}{2} = n.$$

Meanwhile, for  $\theta \in \mathcal{F}_{\theta^*}(\gamma)$ , we consider the norm  $\|\theta\|_{\mathcal{F}} \triangleq \sqrt{\langle \theta, \theta \rangle_{\mathcal{F}}}$  induced by the inner product that characterizes  $\mathcal{F}_{\theta}$ , with the associated dual norm  $\|\cdot\|_{\mathcal{F},*}$ . We use a mirror map  $\varphi_{\theta} : \mathcal{F}_{\theta} \rightarrow \mathbb{R}$  such that  $\varphi_{\theta}(\theta) = \frac{1}{2} \|\theta - \theta^*\|_{\mathcal{F}}^2$ . By observing that

$$D_{\varphi_{\theta}}(\theta, \theta') = \frac{1}{2} \|\theta - \theta'\|_{\mathcal{F}}^2 \quad \forall \theta, \theta' \in \mathcal{F}.$$

we have  $\varphi_{\theta}$  being 1-strongly convex with respect to  $\|\cdot\|_{\mathcal{F}}$ . With the gradient of  $\varphi_{\theta}$ ,  $\nabla \varphi_{\theta}(\theta) = \theta - \theta^*$ , and that of its Fenchel dual  $\nabla \varphi_{\theta}^*(g) = g + \theta^*$ , at the  $(t+1)$ -th iteration, we have

$$\theta_{t+1} = \nabla \varphi_{\theta}^* \left( \nabla \varphi_{\theta}(\theta_t) - \eta_{\theta} \cdot \nabla_{\theta} \widehat{L}_{i_t}^{\text{WAC}}(\theta_t, \mathbf{B}_{t+1}) \right) = \theta_t - \eta_{\theta} \cdot \nabla_{\theta} \widehat{L}_{i_t}^{\text{WAC}}(\theta_t, \mathbf{B}_{t+1}).$$

For  $i_t \sim [n]$  uniformly, the stochastic gradient with respect to  $f$  satisfies that

$$\mathbb{E}_{i_t \sim [n]} \left[ \left\| \nabla_{\theta} \widehat{L}_{i_t}^{\text{WAC}}(\theta_t, \mathbf{B}_{t+1}) \right\|_{\mathcal{F},*}^2 \right] = \frac{1}{n} \sum_{i_t=1}^n \left\| \nabla_{\theta} \widehat{L}_{i_t}^{\text{WAC}}(\theta_t, \mathbf{B}_{t+1}) \right\|_{\mathcal{F},*}^2 \leq C_{\theta,*}^2.$$

Further, in light of the definition of  $\mathcal{F}_{\theta^*}(\gamma)$ , since  $\theta^* \in \mathcal{F}_{\theta^*}(\gamma)$ , with  $\theta^* = \operatorname{argmin}_{\theta \in \mathcal{F}_{\theta^*}(\gamma)} \varphi_{\theta}(\theta)$  and  $\theta' = \operatorname{argmax}_{\theta \in \mathcal{F}_{\theta^*}(\gamma)} \varphi_{\theta}(\theta)$ , we have

$$R_{\mathcal{F}_{\theta^*}(\gamma)}^2 \triangleq \max_{\theta \in \mathcal{F}_{\theta^*}(\gamma)} \varphi_{\theta}(\theta) - \min_{\theta \in \mathcal{F}_{\theta^*}(\gamma)} \varphi_{\theta}(\theta) = \frac{1}{2} \|\theta' - \theta^*\|_{\mathcal{F}}^2 \leq \frac{\gamma^2}{2}.$$

Finally, leveraging Lemma 1 completes the proof.  $\square$

We recall the standard convergence guarantee for online mirror descent on saddle point problems. In general, we consider a stochastic function  $F : \mathcal{U} \times \mathcal{V} \times \mathcal{I} \rightarrow \mathbb{R}$  with the randomness of  $F(u, v; i)$  on  $i \in \mathcal{I}$ . Overloading notation  $\mathcal{I}$  both as the distribution of  $i$  and as the support, we are interested in solving the saddle point problem on the expectation function

$$\min_{u \in \mathcal{U}} \max_{v \in \mathcal{V}} f(u, v) \quad \text{where} \quad f(u, v) \triangleq \mathbb{E}_{i \sim \mathcal{I}} [F(u, v; i)]. \quad (12)$$

**Assumption 2.** Assume that the stochastic objective satisfies the following:

- (i) For every  $i \in \mathcal{I}$ ,  $F(\cdot, v, i)$  is convex for all  $v \in \mathcal{V}$  and  $F(u, \cdot, i)$  is concave for all  $u \in \mathcal{U}$ .
- (ii) The stochastic subgradients  $G_u(u, v; i) \in \partial_u F(u, v; i)$  and  $G_v(u, v; i) \in \partial_v F(u, v; i)$  with respect to  $u$  and  $v$  evaluated at any  $(u, v) \in \mathcal{U} \times \mathcal{V}$  provide unbiased estimators for some respective subgradients of the expectation function: for any  $(u, v) \in \mathcal{U} \times \mathcal{V}$ , there exist some  $g_u(u, v) \triangleq \mathbb{E}_{i \sim \mathcal{I}} [G_u(u, v; i)] \in \partial_u f(u, v)$  and  $g_v(u, v) \triangleq \mathbb{E}_{i \sim \mathcal{I}} [G_v(u, v; i)] \in \partial_v f(u, v)$ .
- (iii) Let  $\|\cdot\|_{\mathcal{U}}$  and  $\|\cdot\|_{\mathcal{V}}$  be arbitrary norms that are well-defined on  $\mathcal{U}$  and  $\mathcal{V}$ , while  $\|\cdot\|_{\mathcal{U},*}$  and  $\|\cdot\|_{\mathcal{V},*}$  be their respective dual norms. There exist constants  $C_{u,*}, C_{v,*} > 0$  such that

$$\mathbb{E}_{i \sim \mathcal{I}} [\|G_u(u, v; i)\|_{\mathcal{U},*}^2] \leq C_{u,*}^2 \quad \text{and} \quad \mathbb{E}_{i \sim \mathcal{I}} [\|G_v(u, v; i)\|_{\mathcal{V},*}^2] \leq C_{v,*}^2 \quad \forall (u, v) \in \mathcal{U} \times \mathcal{V}.$$

For online mirror descent, we further introduce two mirror maps that induce distances on  $\mathcal{U}$  and  $\mathcal{V}$ , respectively.

**Assumption 3.** Let  $\varphi_u : \mathcal{D}_u \rightarrow \mathbb{R}$  and  $\varphi_v : \mathcal{D}_v \rightarrow \mathbb{R}$  satisfy the following:

- (i)  $\mathcal{U} \subseteq \mathcal{D}_u \cup \partial \mathcal{D}_u$ ,  $\mathcal{U} \cap \mathcal{D}_u \neq \emptyset$  and  $\mathcal{V} \subseteq \mathcal{D}_v \cup \partial \mathcal{D}_v$ ,  $\mathcal{V} \cap \mathcal{D}_v \neq \emptyset$ .
- (ii)  $\varphi_u$  is  $\rho_u$ -strongly convex with respect to  $\|\cdot\|_{\mathcal{U}}$ ;  $\varphi_v$  is  $\rho_v$ -strongly convex with respect to  $\|\cdot\|_{\mathcal{V}}$ .
- (iii)  $\lim_{u \rightarrow \partial \mathcal{D}_u} \|\nabla \varphi_u(u)\|_{\mathcal{U},*} = \lim_{v \rightarrow \partial \mathcal{D}_v} \|\nabla \varphi_v(v)\|_{\mathcal{V},*} = +\infty$ .

Given the learning rates  $\eta_u, \eta_v$ , in each iteration  $t = 1, \dots, T$ , the online mirror descent samples  $i_t \sim \mathcal{I}$  and updates

$$\begin{aligned} v_{t+1} &= \operatorname{argmin}_{v \in \mathcal{V}} -\eta_v \cdot G_v(u_t, v_t; i_t)^\top v + D_{\varphi_v}(v, v_t), \\ u_{t+1} &= \operatorname{argmin}_{u \in \mathcal{U}} \eta_u \cdot G_u(u_t, v_{t+1}; i_t)^\top u + D_{\varphi_u}(u, u_t), \end{aligned} \quad (13)$$

where  $D_{\varphi}(w, w') = \varphi(w) - \varphi(w') - \nabla \varphi(w')^\top (w - w')$  denotes the Bregman divergence.

We measure the convergence of the saddle point problem in the duality gap:

$$\mathcal{E}(\bar{u}_T, \bar{v}_T) \triangleq \max_{v \in \mathcal{V}} f(\bar{u}_T, v) - \min_{u \in \mathcal{U}} f(u, \bar{v}_T)$$

such that, with

$$R_{\mathcal{U}} \triangleq \sqrt{\max_{u \in \mathcal{U} \cap \mathcal{D}_u} \varphi_u(u) - \min_{u \in \mathcal{U} \cap \mathcal{D}_u} \varphi_u(u)} \quad \text{and} \quad R_{\mathcal{V}} \triangleq \sqrt{\max_{v \in \mathcal{V} \cap \mathcal{D}_v} \varphi_v(v) - \min_{v \in \mathcal{V} \cap \mathcal{D}_v} \varphi_v(v)},$$

the online mirror descent converges as follows.

**Lemma 1** ([Nemirovski et al., 2009] (3.11)). *Under Assumption 2 and Assumption 3, when taking constant learning rates  $\eta_u = \eta_v = 2 / \sqrt{5T \left( \frac{2R_u^2}{\rho_u} C_{u,*}^2 + \frac{2R_v^2}{\rho_v} C_{v,*}^2 \right)}$ , with  $\bar{u}_T = \frac{1}{T} \sum_{t=1}^T u_t$  and  $\bar{v}_T = \frac{1}{T} \sum_{t=1}^T v_t$ ,*

$$\mathbb{E} [\mathcal{E} (\bar{u}_T, \bar{v}_T)] \leq 2 \sqrt{\frac{10 \left( \rho_v R_u^2 C_{u,*}^2 + \rho_u R_v^2 C_{v,*}^2 \right)}{\rho_u \rho_v \cdot T}}.$$

**Example 1** (Binary linear pixel-wise classifiers with convex and continuous objectives). We consider a pixel-wise binary classification problem with  $\mathcal{X} = [0, 1]^d$ , augmentations  $A : \mathcal{X} \rightarrow \mathcal{X}$  for all  $A \sim \mathcal{A}$ , and a class of linear “UNets”,

$$\mathcal{F} = \left\{ f_\theta : \mathcal{X} \rightarrow [0, 1]^d \mid f_\theta(\mathbf{x}) = \sigma \left( \boldsymbol{\theta}_d \boldsymbol{\theta}_e^\top \mathbf{x} \right) = \psi_\theta(\phi_\theta(\mathbf{x})), \phi_\theta(\mathbf{x}) = \frac{1}{\sqrt{d}} \boldsymbol{\theta}_e^\top \mathbf{x} \right\},$$

where the parameter space  $\theta = (\boldsymbol{\theta}_e, \boldsymbol{\theta}_d) \in \mathcal{F}_\theta = \mathbb{S}^{d-1} \times \mathbb{S}^{d-1}$  is equipped with the  $\ell_2$  norm  $\|\theta\|_{\mathcal{F}} = \left( \|\boldsymbol{\theta}_e\|_2^2 + \|\boldsymbol{\theta}_d\|_2^2 \right)^{1/2}$ ;  $\sigma : \mathbb{R}^d \rightarrow [0, 1]^d$  denotes entry-wise application of the sigmoid function  $\sigma(z) = (1 + e^{-z})^{-1}$ ; and the latent space of encoder outputs  $(\mathcal{Z}, \varrho)$  is simply the real line. Given the data distribution  $P_\xi$ , we recall that  $\theta^* = \operatorname{argmin}_{\theta \in \mathcal{F}_\theta} \mathbb{E}_{(\mathbf{x}, \mathbf{y}) \sim P_\xi} [\ell_{CE}(\theta; (\mathbf{x}, \mathbf{y}))]$  for all  $\xi \in [0, 1]$  and let  $\mathcal{F}_{\theta^*}(\gamma) = \{\theta \in \mathcal{F}_\theta \mid \|\theta - \theta^*\|_{\mathcal{F}} \leq \gamma\}$  for some  $\gamma = O(1/\sqrt{d})$ . We assume that  $|\mathbf{x}^\top \boldsymbol{\theta}_e^*| = O(1)$  for all  $\mathbf{x} \in \mathcal{X}$ . Then,  $\ell_{CE}(\theta; (\mathbf{x}, \mathbf{y}))$  and  $\ell_{AC}(\theta; \mathbf{x}, A_1, A_2)$  are convex and continuous in  $\theta$  for all  $(\mathbf{x}, \mathbf{y}) \in \mathcal{X} \times [K]^d$ ,  $A_1, A_2 \sim \mathcal{A}^2$ ; while  $C_{\theta,*} \leq \max(2\sqrt{2}, 2\lambda_{AC})$  and  $C_{\beta,*} \leq \max(O(1), 2\lambda_{AC})$ .

*Rationale for Example 1.* Let  $\mathbf{y}_k = \mathbb{I}\{\mathbf{y} = k\}$  entry-wise for  $k = 0, 1$ . We would like to show that, for any given  $(\mathbf{x}, \mathbf{y}) \in \mathcal{X} \times [K]^d$ ,  $A_1, A_2 \sim \mathcal{A}^2$ ,

$$\begin{aligned} \ell_{CE}(\theta) &= -\frac{1}{d} \left( \mathbf{y}_1^\top \log \sigma \left( \boldsymbol{\theta}_d \boldsymbol{\theta}_e^\top \mathbf{x} \right) + \mathbf{y}_0^\top \log \sigma \left( -\boldsymbol{\theta}_d \boldsymbol{\theta}_e^\top \mathbf{x} \right) \right), \\ \ell_{AC}(\theta) &= \frac{\lambda_{AC}}{\sqrt{d}} \cdot (A_1(\mathbf{x}) - A_2(\mathbf{x}))^\top \boldsymbol{\theta}_e \end{aligned}$$

are convex and continuous in  $\theta = (\boldsymbol{\theta}_e, \boldsymbol{\theta}_d)$ .

First, we observe that  $\ell_{AC}(\theta)$  is linear (and therefore convex and continuous) in  $\theta$  for all  $\mathbf{x} \in \mathcal{X}$ ,  $A_1, A_2 \sim \mathcal{A}^2$ , with

$$\nabla_{\boldsymbol{\theta}_e} \ell_{AC}(\theta) = \frac{\lambda_{AC}}{\sqrt{d}} \cdot (A_1(\mathbf{x}) - A_2(\mathbf{x})), \quad \nabla_{\boldsymbol{\theta}_d} \ell_{AC}(\theta) = \mathbf{0}$$

such that  $\|\nabla_{\theta} \ell_{AC}(\theta)\|_{\mathcal{F},*} \leq 2\lambda_{AC}$ .

Meanwhile, with  $\mathbf{z}(\theta) = \boldsymbol{\theta}_d \boldsymbol{\theta}_e^\top \mathbf{x}$ , we have  $\ell_{CE}(\theta) = -\frac{1}{d} (\mathbf{y}_1^\top \log \sigma(\mathbf{z}(\theta)) + \mathbf{y}_0^\top \log \sigma(-\mathbf{z}(\theta)))$  being convex and continuous in  $\mathbf{z}(\theta)$ :

$$\nabla_{\mathbf{z}}^2 \ell_{CE}(\theta) = \frac{1}{d} \operatorname{diag}(\sigma(\mathbf{z}(\theta))) \operatorname{diag}(1 - \sigma(\mathbf{z}(\theta))) \succcurlyeq 0.$$

Therefore,  $\ell_{CE}(\theta)$  is convex and continuous in  $\theta$  for all  $(\mathbf{x}, \mathbf{y}) \in \mathcal{X} \times [K]^d$ :

$$\underbrace{\nabla_{\theta}^2 \ell_{CE}(\theta)}_{2d \times 2d} = \begin{bmatrix} \mathbf{x} \boldsymbol{\theta}_d^\top \\ (\boldsymbol{\theta}_e^\top \mathbf{x}) \mathbf{I}_d \end{bmatrix} \left( \frac{1}{d} \operatorname{diag}(\sigma(\mathbf{z}(\theta))) \operatorname{diag}(1 - \sigma(\mathbf{z}(\theta))) \right) \begin{bmatrix} \mathbf{x} \boldsymbol{\theta}_d^\top & (\boldsymbol{\theta}_e^\top \mathbf{x}) \mathbf{I}_d \end{bmatrix} \succcurlyeq 0,$$



where  $\mathbf{I}_d$  denotes the  $d \times d$  identity matrix. Further, from the derivation, we have

$$\nabla_{\boldsymbol{\theta}_e} \ell_{CE}(\boldsymbol{\theta}) = \frac{1}{d} \boldsymbol{\theta}_d^\top \left( \sigma \left( \boldsymbol{\theta}_d \boldsymbol{\theta}_e^\top \mathbf{x} \right) - \mathbf{y} \right) \mathbf{x}, \quad \nabla_{\boldsymbol{\theta}_d} \ell_{CE}(\boldsymbol{\theta}) = \frac{\boldsymbol{\theta}_e^\top \mathbf{x}}{d} \left( \sigma \left( \boldsymbol{\theta}_d \boldsymbol{\theta}_e^\top \mathbf{x} \right) - \mathbf{y} \right)$$

such that  $\|\nabla_{\boldsymbol{\theta}} \ell_{CE}(\boldsymbol{\theta})\|_{\mathcal{F},*} = \sqrt{\|\nabla_{\boldsymbol{\theta}_e} \ell_{CE}(\boldsymbol{\theta})\|_2^2 + \|\nabla_{\boldsymbol{\theta}_d} \ell_{CE}(\boldsymbol{\theta})\|_2^2} \leq 2\sqrt{2}$ .

Finally, knowing  $\|\nabla_{\boldsymbol{\theta}} \ell_{CE}(\boldsymbol{\theta})\|_{\mathcal{F},*} \leq 2\sqrt{2}$  and  $\|\nabla_{\boldsymbol{\theta}} \ell_{AC}(\boldsymbol{\theta})\|_{\mathcal{F},*} \leq 2\lambda_{AC}$ , we have

$$\left\| \nabla_{\boldsymbol{\theta}} \widehat{L}_i^{WAC}(\boldsymbol{\theta}, \boldsymbol{\beta}) \right\|_{\mathcal{F},*} \leq \beta_{[i]} \|\nabla_{\boldsymbol{\theta}} \ell_{CE}(\boldsymbol{\theta})\|_{\mathcal{F},*} + (1 - \beta_{[i]}) \|\nabla_{\boldsymbol{\theta}} \ell_{AC}(\boldsymbol{\theta})\|_{\mathcal{F},*} \leq \max(2\sqrt{2}, 2\lambda_{AC})$$

for all  $i \in [n]$ , and therefore,

$$C_{\boldsymbol{\theta},*} \leq \max(2\sqrt{2}, 2\lambda_{AC}).$$

Besides, with

$$\ell_{AC}(\boldsymbol{\theta}) \leq \frac{\lambda_{AC}}{\sqrt{d}} \|A_1(\mathbf{x}) - A_2(\mathbf{x})\|_2 \|\boldsymbol{\theta}_e\|_2 \leq 2\lambda_{AC},$$

and since

$$\begin{aligned} \left( \boldsymbol{\theta}_d \boldsymbol{\theta}_e^\top \mathbf{x} \right)_{[j]} &\leq \left| \mathbf{x}^\top \boldsymbol{\theta}_e \right| \leq \left| \mathbf{x}^\top (\boldsymbol{\theta}_e - \boldsymbol{\theta}_e^*) \right| + \left| \mathbf{x}^\top \boldsymbol{\theta}_e^* \right| \leq \|\mathbf{x}\|_2 \|\boldsymbol{\theta}_e - \boldsymbol{\theta}_e^*\|_2 + O(1) \\ &\leq \gamma \sqrt{d} + O(1) = O(1) \end{aligned}$$

for all  $j \in [d]$ ,  $\ell_{CE}(\boldsymbol{\theta}) \leq \log(1 + e^{O(1)}) = O(1)$ , we have

$$C_{\boldsymbol{\beta},*} \leq \max(O(1), 2\lambda_{AC}).$$

□

## C Dice Loss for Pixel-wise Class Imbalance

With finite samples in practice, since the averaged cross-entropy loss (Equation (2)) weights each pixel in the image label equally, the pixel-wise class imbalance can become a problem. For example, the background pixels can be dominant in most of the segmentation labels, making the classifier prone to predict pixels as background.

To cope with such vulnerability, [Cao et al. \[2021\]](#), [Chen et al. \[2021\]](#), [Taghanaki et al. \[2019b\]](#), [Wong et al. \[2018\]](#), [Yeung et al. \[2022\]](#) propose to combine the cross-entropy loss with the *dice loss*—a popular segmentation loss based on the overlap between true labels and their corresponding predictions in each class:

$$\ell_{DICE}(\boldsymbol{\theta}; (\mathbf{x}, \mathbf{y})) = 1 - \frac{1}{K} \sum_{k=1}^K DSC \left( f_{\boldsymbol{\theta}}(\mathbf{x})_{[:,k]}, \mathbb{I}\{\mathbf{y} = k\} \right), \quad (14)$$

where for any  $\mathbf{p} \in [0, 1]^d$ ,  $\mathbf{q} \in \{0, 1\}^d$ ,  $DSC(\mathbf{p}, \mathbf{q}) = \frac{2\mathbf{p}^\top \mathbf{q}}{\|\mathbf{p}\|_1 + \|\mathbf{q}\|_1} \in [0, 1]$  denotes the dice coefficient [\[Milletari et al., 2016, Taghanaki et al., 2019a\]](#). Notice that by measuring the bounded dice coefficient for each of the  $K$  classes individually, the dice loss tends to be robust to class imbalance.

Taghanaki et al. [2019b] merges both dice and averaged cross-entropy losses via a convex combination. It is also a common practice to add a smoothing term in both the nominator and denominator of the DSC [Russell and Norvig, 2016].

Combining the dice loss (Equation (14)) with the weighted augmentation consistency regularization formulation (Equation (5)), in practice, we solve

$$\begin{aligned} \hat{\theta}^{WAC}, \hat{\beta} \in \underset{\theta \in \mathcal{F}_{\theta^*}(\gamma)}{\operatorname{argmin}} \underset{\beta \in [0,1]^n}{\operatorname{argmax}} \left\{ \hat{L}^{WAC}(\theta, \beta) \triangleq \frac{1}{n} \sum_{i=1}^n \hat{L}_i^{WAC}(\theta, \beta) \right\} \\ \hat{L}_i^{WAC}(\theta, \beta) \triangleq \ell_{DICE}(\theta; (\mathbf{x}_i, \mathbf{y}_i)) + \beta_{[i]} \cdot \ell_{CE}(\theta; (\mathbf{x}_i, \mathbf{y}_i)) + (1 - \beta_{[i]}) \cdot \ell_{AC}(\theta; \mathbf{x}_i, A_{i,1}, A_{i,2}) \end{aligned} \quad (15)$$

with a slight modification in Algorithm 1 line 9:

$$\begin{aligned} \theta_t \leftarrow \theta_{t-1} - \eta_{\theta} \cdot \left( \nabla_{\theta} \ell_{DICE}(\theta_{t-1}; (\mathbf{x}_{i_t}, \mathbf{y}_{i_t})) + (\beta_t)_{[i_t]} \cdot \nabla_{\theta} \ell_{CE}(\theta_{t-1}; (\mathbf{x}_{i_t}, \mathbf{y}_{i_t})) \right. \\ \left. + \left( 1 - (\beta_t)_{[i_t]} \right) \cdot \nabla_{\theta} \ell_{AC}(\theta_{t-1}; \mathbf{x}_{i_t}, A_{i_t,1}, A_{i_t,2}) \right). \end{aligned}$$

**On the influence of incorporating dice loss in experiments.** We note that, in the experiments, the dice loss  $\ell_{DICE}$  is treated independently of *AdaWAC* in Algorithm 1 via standard stochastic gradient descent. In particular for the comparison with hard thresholding algorithms in Table 2, we keep the updating on  $\ell_{DICE}$  of the original untrimmed batch intact for both **trim-train** and **trim-ratio** to exclude the potential effect of  $\ell_{DICE}$  that is not involved in reweighting.

## D Implementation Details and Datasets

We use the official implementation of TransUNet<sup>10</sup> for model training. We use the same optimizer (SGD with learning rate 0.01, momentum 0.9, and weight decay 1e-4). For the learning rate schedule, we follow the polynomial learning rate decay for the original TransUNet baseline and use a constant learning rate for *AdaWAC*. For the Synapse dataset, we train TransUNet for 14k iterations on the training dataset and evaluate the last-iteration model on the test dataset; for the ACDC dataset, we train TransUNet for 20k iterations, validate models on the validation dataset every 500 iterations for baseline (every 560 iterations, i.e., 10 epochs for *AdaWAC*), and test on the best model selected by the validation dataset. The total training iterations are set the same as that in vanilla TransUNet [Chen et al., 2021].

**Synapse multi-organ segmentation dataset (Synapse).** The Synapse dataset<sup>11</sup> is a multi-organ abdominal CT scans for medical image segmentation in the MICCAI 2015 Multi-Atlas Abdomen Labelling Challenge [Chen et al., 2021]. There are 30 volumetric CT scans with variable volume sizes ( $512 \times 512 \times 85 - 512 \times 512 \times 198$ ), and slice thickness ranges from 2.5mm to 5.0mm. We use the pre-processed data provided by Chen et al. [2021] and follow their train/test split to use 18 volumes for training and 12 volumes for testing on 8 abdominal organs—aorta, gallbladder, left kidney (L), right kidney (R), liver, pancreas, spleen, and stomach. The abdominal organs were labeled by experience undergraduates and verified by a radiologist using MIPAV software according to the information from Synapse wiki page.

<sup>10</sup><https://github.com/Beckschen/TransUNet>

<sup>11</sup>See detailed description at <https://www.synapse.org/#!Synapse:syn3193805/wiki/217789>

**Automated cardiac diagnosis challenge dataset (ACDC).** The ACDC dataset<sup>12</sup> is cine-MRI scans in the MICCAI 2017 Automated Cardiac Diagnosis Challenge. There are 200 scans from 100 patients, and each patient has two volumetric frames with slice thickness from 5mm to 8mm. We use the pre-processed data also provided by Chen et al. [2021] and follow their train/validate/test split to use 70 patients’ scans for training, 10 patients’ scans for validation, and 20 patients’ scans for testing on three cardiac structures—left ventricle (LV), myocardium (MYO), and right ventricle (RV). The data were labeled by one clinical expert according to the description on ACDC dataset website.

## E Additional Results

### E.1 Visualization of segmentation on ACDC dataset

As shown in Figure 4, the model trained by *AdaWAC* segments cardiac structures with more accurate shapes (column 1), identifies organs missed by baseline TransUNet (column 2-3) and circumvents the false-positive pixel classifications (*i.e.*, fake predictions of background pixels as organs) suffered by the TransUNet baseline (column 4-6).

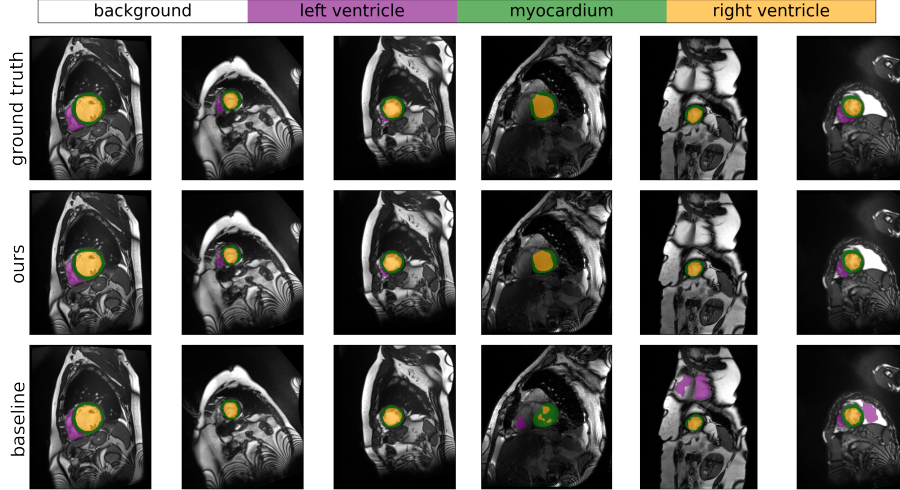


Figure 4: Visualization of segmentation results on ACDC dataset. From top to bottom: ground truth, ours, and baseline method.

### E.2 Experimental Results on Previous Metrics

In this section, we include the results of experiments on Synapse<sup>13</sup> dataset with metrics defined in TransUNet [Chen et al., 2021] for reference. In TransUNet [Chen et al., 2021], DSC is 1 when the sum of ground truth labels is zero (*i.e.*,  $gt.sum() == 0$ ) while the sum of predicted labels is nonzero (*i.e.*,  $pred.sum() > 0$ ). However, according to the definition of dice scores,  $DSC = 2|A \cap B|/(|A| + |B|)$ ,  $\forall A, B$ , the DSC for the above case should be 0 since the intersection is 0 and the denominator is non-zero. In our evaluation, we change the special condition for DSC as 1 to  $pred.sum == 0$  and  $gt.sum() == 0$  instead, in which case the denominator is 0.

<sup>12</sup>See detailed description at <https://www.creatis.insa-lyon.fr/Challenge/acdc/>

<sup>13</sup>Note that the numbers of correct metrics and metrics in TransUNet [Chen et al., 2021] on ACDC dataset are the same.

Table 5: Ablation study on Synapse with metrics in TransUNet [Chen et al., 2021].

Method	DSC $\uparrow$	HD95 $\downarrow$	Aorta	Gallbladder	Kidney (L)	Kidney (R)	Liver	Pancreas	Spleen	Stomach
baseline	77.32	29.23	87.46	63.54	82.06	77.76	94.10	54.06	85.07	74.54
reweight-only	77.72	29.24	86.15	62.31	82.96	80.28	93.42	55.86	85.29	75.49
ACR-only	78.93	31.65	87.96	62.67	81.79	80.21	94.52	60.41	88.07	75.83
AdaWAC-0.01	78.98	27.81	87.58	61.09	82.29	80.22	94.90	55.92	91.63	78.23
AdaWAC-1.0	80.16	25.79	87.23	63.27	84.58	81.69	94.62	58.29	90.63	81.01

Table 6: Sample efficiency on Synapse with metrics in TransUNet [Chen et al., 2021].

Training	Method	DSC $\uparrow$	HD95 $\downarrow$	Aorta	Gallbladder	Kidney (L)	Kidney (R)	Liver	Pancreas	Spleen	Stomach
full	baseline	77.32	29.23	87.46	63.54	82.06	77.76	94.10	54.06	85.07	74.54
	AdaWAC	80.16	25.79	87.23	63.27	84.58	81.69	94.62	58.29	90.63	81.01
half-vol	baseline	72.65	35.86	83.29	43.70	78.25	77.25	92.92	51.32	83.80	70.66
	AdaWAC	75.93	34.95	84.45	60.40	79.59	76.06	93.19	54.46	84.91	74.37
half-slice	baseline	76.24	24.66	86.26	57.61	79.32	76.55	94.34	54.04	86.20	75.57
	AdaWAC	78.14	29.75	86.66	62.28	81.36	78.84	94.60	57.95	85.38	78.01
half-sparse	baseline	0.00	0.00	0.00	0.00	0.00	0.00	0.00	0.00	0.00	0.00
	AdaWAC	39.68	80.93	76.59	0.00	66.53	62.11	49.69	31.09	12.30	19.11

Table 7: Comparison with trimmed-loss methods on Synapse with metrics in TransUNet [Chen et al., 2021].

Method	DSC $\uparrow$	HD95 $\downarrow$	Aorta	Gallbladder	Kidney (L)	Kidney (R)	Liver	Pancreas	Spleen	Stomach
baseline	77.32	29.23	87.46	63.54	82.06	77.76	94.10	54.06	85.07	74.54
trim-train	77.05	26.94	86.70	60.65	80.02	76.64	94.25	54.20	86.44	77.49
trim-ratio	75.30	28.59	87.35	57.29	78.70	72.22	94.18	52.32	86.31	74.03
trim-train+ACR	76.70	35.06	87.11	62.22	74.19	75.25	92.19	57.16	88.21	77.30
trim-ratio+ACR	79.02	33.59	86.82	61.67	83.52	81.22	94.07	59.06	88.08	77.71
AdaWAC (ours)	80.16	25.79	87.23	63.27	84.58	81.69	94.62	58.29	90.63	81.01